Measurement 259 (2026) 119624

Contents lists available at ScienceDirect

Measurement

journal homepage: www.elsevier.com/locate/measurement

Liquid particle monitoring system utilizing aerosol metrology and data processing algorithm: chemical mechanical polishing slurry application

Seongmin Cho [a], Yongjae Cho [a], Yusun Lee [a], Seungjae Gwak [a], Heedo Seo [b], Su Bin Min [b], Young June Won [b], Jung-Hun Noh [c], Handol Lee [d], Dong-Bin Kwak [a,*]

[a] Department of Manufacturing Systems and Design Engineering, Seoul National University of Science and Technology, 232 Gongneung-ro, Nowon-gu, Seoul 01811, Republic of Korea
[b] EHS/Infra Technology Research Center, Samsung Electronics Co., Ltd., Samsungjeonja-ro 1, Hwaseong-si 18448, Republic of Korea
[c] Mechanical Convergence System Center, Institute for Advanced Engineering, 175-28, Goan-ro 51 beon-gil, Baegam-myeon, Cheoin-gu, Yongin-si, Gyeonggi-do 17180, Republic of Korea
[d] Department of Environmental Engineering, Inha University, 100 Inha-ro, Michuhol-gu, Incheon 22212, Republic of Korea

ARTICLE INFO

Keywords:
Aerosol metrology
Atomizer-SMPS
Hydrosol Particle Size Distribution
Non-volatile Residue
Aerosol-to-Hydrosol Inversion

ABSTRACT

This study presents an aerosol-metrology approach using an integrated atomizer–SMPS (A-SMPS) to measure NVR-subtracted hydrosol particle size distributions (HPSDs). Standard polystyrene latex (PSL) nanospheres and three chemical mechanical polishing (CMP) slurries (two silica-based and one ceria-based) were measured with the A-SMPS. A multi-stage algorithm converts the SMPS-measured aerosol particle size distribution (ASD) into an NVR-subtracted hydrosol particle size distribution by sequentially (i) removing non-volatile residues (NVRs) generated during aerosolization to yield the NVR-subtracted aerosol particle size distribution and (ii) applying an empirically derived calibration based on PSL references. Experimental results indicate that this approach yields consistent HPSDs across different dilution factors (DFs), effectively separating abrasive particle peaks from surfactant-induced NVR peaks. For the ceria and two silica slurries, the peak positions and amplitudes were nearly invariant across DFs confirming the robustness of the ASD-to-HPSD inversion and the accuracy of the DF-corrected original number concentrations. Integrating aerosol-based detection with the inversion process offers a precise and flexible strategy for quantifying ~ 100 nm abrasive particles in CMP slurries, and enables accurate hydrosol characterization for semiconductor process optimization.

1. Introduction

The contemporary scientific and industrial realms have been propelled forward by the advent of nanoscale science, which encompasses the engineering of nanoparticles. The transition from micro to nanoscale particle technology has resulted in the application of a multitude of engineered nanomaterials across a diverse range of fields, including materials science, chemical engineering, energy systems, environmental technologies, healthcare, and semiconductor fabrication [1–6]. A comprehensive understanding of the properties and characteristics of nanoparticles is essential for their optimal utilization. Accurate characterization, encompassing the measurement of number concentration and particle size distribution (PSD), is vital for enhancing performance and mitigating potential risks. This is particularly crucial in fields such as healthcare, environmental management, and microchip fabrication, where precision and safety are of paramount importance [7–9].

Chemical Mechanical Polishing (CMP) is an essential process in semiconductor manufacturing, used to achieve globally and locally planar wafer surfaces for subsequent devices. In CMP, a liquid slurry containing fine abrasive particles (commonly nanoscale oxides such as colloidal silica or ceria) and reactive chemicals is applied between a polishing pad and the wafer surface [10]. Slurry abrasives, together with chemical reactions, remove material in a controlled manner to produce a flat surface. Crucially, the size distribution of these abrasive particles must be tightly controlled, as it directly impacts both polishing performance and defect.

One well-known issue in CMP is the formation of micro-scratches on the wafer, which has long been attributed to the presence of oversized particles in the slurry. Even a small number of large particles or agglomerates can introduce significant scratching and surface defects. CMP-induced defect studies have linked small populations of over 500

* Corresponding author.
E-mail address: dbkwak@seoultech.ac.kr (D.-B. Kwak).

https://doi.org/10.1016/j.measurement.2025.119624
Received 15 July 2025; Received in revised form 24 October 2025; Accepted 4 November 2025
Available online 5 November 2025

Nomenclature

CMP	Chemical mechanical polishing
A-SMPS	Atomizer-Scanning mobility particle sizer
ASD	Aerosol particle size distribution
APSD	NVR-subtracted aerosol particle size distribution
HSD	Hydrosol particle size distribution
HPSD	NVR-subtracted hydrosol particle size distribution
DF	Dilution factor
1/DF	Fractional concentration
D_p	Particle mobility diameter
N_A	Aerosol particle number concentration
N_H	Hydrosol particle number concentration
N_{AP}	NVR-subtracted aerosol particle number concentration
N_{HP}	NVR-subtracted hydrosol particle number concentration
DF × N_{HP}	DF-corrected original number concentration
$dN_A/d\log_{10}D_p$	Aerosol particle size distribution (ASD)
$dN_H/d\log_{10}D_p$	Hydrosol particle size distribution (HSD)
$dN_{AP}/d\log_{10}D_p$	NVR-subtracted aerosol particle size distribution (APSD)
$dN_{HP}/d\log_{10}D_p$	NVR-subtracted hydrosol particle size distribution (HPSD)
DF × $dN_{HP}/d\log_{10}D_p$	DF-corrected HPSD
A_j	Mode amplitude of the j^{th} log-normal mode
μ_j	Geometric mean diameter of the j^{th} log-normal mode
σ_j	Geometric standard deviation of the j^{th} log-normal mode
μ_{rep}	Particle representative mean diameter
$D_{p,\ Cutoff}$	Boundary for NVR and particle classification
CV	Coefficient of Variation

nm sized particles in the slurry to increased scratch counts on polished wafers [11]. Under high-shear CMP conditions, slurry particles can agglomerate into larger clusters; such shear-induced large particles (≥ 300 nm) have been shown to cause dramatic spikes in scratching. In one study, a slurry that underwent shear thickening (forming a minor fraction of ≥ 300 nm agglomerates) produced about seven times more surface scratches than a well-dispersed slurry, underscoring how detrimental even a few large particles can be [11]. Accordingly, removing or preventing these oversized particles greatly reduces the occurrence of defects. In practice, installing fine filters to eliminate particles above a certain threshold (e.g. 200 to 500 nm) has been found to markedly cut down scratch defects without harming CMP performance [10]. Indeed, modern CMP operations rely on rigorous slurry quality control – including continuous particle size monitoring and filtration – to ensure the delivered slurry is free of large agglomerates and contaminants, thereby minimizing scratches and maintaining high yield. These requirements motivate the development of advanced particle-monitoring techniques for CMP.

A variety of conventional methods are employed to quantify and characterize hydrosols (i.e., liquid-borne particles within liquid solutions). These include optical-based techniques such as the Liquid Particle Counter (LPC) and the Dynamic Light Scattering (DLS) method [9,12–18]. LPC employs optical-based methods to detect and quantify particle sizes and concentrations in liquids, thereby providing real-time monitoring for nanoparticle detection. Although LPC is a widely used technique in the semiconductor and pharmaceutical industries, it has certain limitations when analyzing liquid-borne nanoparticles according to prior studies [17,19,20]. The phenomenon of optical coincidence, whereby multiple particles are misclassified as a single entity, results in an underestimation of concentration in high-concentration solutions [19]. Specifically, the reliance of LPC on calibration with standard particles, such as polystyrene latex (PSL) spheres, results in inaccuracies when characterizing target particles, such as silica or ceria, which have distinct refractive indices [21,22]. This dependence on the refractive index may result in the exclusion of particles below 20 ~ 30 nm, thereby limiting the accuracy of detection. This lower detection limit is consistent with the performance specifications of commercially available LPCs, which typically operate above a minimum particle size of 0.02 μm (20 nm). Micro- or nano-bubbles present in the liquid flow during the measurement can be misclassified as particles, representing one of the major factors that reduce the reliability of LPC measurements [23]. As LPCs employ a light-scattering detection principle that cannot distinguish between particles and bubbles, they are in fact frequently utilized in applications aimed at measuring bubble-size distributions in liquids [23,24]. In addition, LPC encounters difficulties when analyzing polydisperse solutions, wherein particles of varying sizes coexist, thereby further complicating measurements. These limitations underscore the necessity for the development of more sophisticated detection technologies.

Moreover, DLS also has notable shortcomings in hydrosol measurements. The intensity-based approach employed by this method results in the overrepresentation of larger particles, which in turn leads to the skewing of size distributions that are critical for accurate polishing performance. The dependence of particle size measurements on refractive index presents additional challenges in the detection of materials with indices approaching that of the medium. Aggregate interference represents another significant hurdle, particularly in the case of stabilized suspensions or those that have been stored for an extended period. Environmental factors, such as temperature and viscosity, also exert a considerable influence on particle diffusion, underscoring the necessity for precise calibration to ensure reliable results [2,18,25].

Aerosol detection techniques, such as the Scanning Mobility Particle Sizer (SMPS), have emerged as pivotal tools for characterizing nanoparticles in a variety of applications, including Chemical Mechanical Polishing (CMP) slurry analysis. The SMPS employs electrical mobility to classify and measure nanoparticles, thereby enabling precise characterization of particle size distributions (PSDs) even in polydisperse and multimodal systems [16,18,26–29]. Prior research has illustrated the efficacy of SMPS in examining hydrosols such as CMP slurries, where precise PSD assessment is vital for process performance and the minimization of surface imperfections in CMP. Among these, the electrospray-SMPS (ES-SMPS) method has been demonstrated to reduce non-volatile residue (NVR) interference, thereby enhancing the clarity of PSD measurements [30]. By converting liquid samples into aerosols, SMPS ensures high-resolution PSD analysis, rendering it especially suitable for monitoring and controlling the properties of advanced CMP slurries [16]. These studies underscore the utility of aerosol-based metrology for both research and industrial applications, thereby paving the way for enhanced nanoparticle characterization and process efficiency in semiconductor manufacturing. However, despite these advances, previous aerosol-based approaches to hydrosol (e.g., CMP slurry) analysis have faced intrinsic limitations. While electrospray-based aerosolization (ES-SMPS) can suppress NVR artifacts by producing very small droplets, its routine use in production settings is constrained by stringent stability requirements such as sustaining a steady Taylor cone and the need to raise solution conductivity via electrolyte doping—steps that complicate inline or in-situ deployment and long-term unattended operation.

Most prior studies measured aerosolized particle data using SMPS, but such measurements only reflected the aerosol-phase concentration—not the true liquid-borne particle concentration originally present in the hydrosol [16,26,30–32]. In other words, aerosol-based characterization provided valuable information on particle size distributions but could not directly quantify the particle number

concentration in the liquid phase. A few follow-up works attempted to address this limitation by converting aerosol data back to hydrosol concentrations through a volume standard–based calibration [16]. However, these methods employed a single-size standard particle, neglecting the size-dependent nature of the aerosol-to-hydrosol relationship. As a result, their calibration was valid only for the reference size used and could not accurately represent real CMP slurries with broad or multimodal particle-size distributions.

In contrast, the atomizer–SMPS (A-SMPS) configuration proposed in this study accepts native slurry formulations without chemical modification and provides robust, continuous sample delivery at practical flow rates, aligning better with the reliability demands of industrial monitoring. This design provides both experimental robustness and compatibility with practical process conditions, ensuring stable aerosol generation even under high particle concentrations. More importantly, this study bridges a long-standing gap in aerosol-based liquid nanoparticle metrology. The proposed A-SMPS framework, integrated with a multi-stage inversion algorithm, not only eliminates NVR interference but also introduces a size-dependent calibration logic that directly connects aerosol-phase measurements to liquid-phase particle concentrations. This dual advancement — namely, the physical separation of NVR and the quantitative reconstruction of the true particle-only distribution — enables accurate retrieval of the solid abrasive particle population within CMP slurries, which conventional optical or aerosol-only methods could not resolve. By establishing this particle size-dependent aerosol-to-hydrosol mapping, the A-SMPS system demonstrates a transformative capability for CMP slurry characterization, providing a path toward real-time, high-fidelity monitoring essential for next-generation semiconductor manufacturing. To situate this capability within current fab practice, a specification-level comparison against instruments actually used for CMP slurry monitoring (at-line DLS, advanced LPCs, and auto dilution SPOS) is provided in Sup. Table S1. In brief, A-SMPS avoids optical-property artifacts, suppresses bubble interference via aerosolization, and uniquely reconstructs hydrosol number concentration from aerosol data at very high slurry concentrations with minimal dilution.

While the proposed A-SMPS framework offers significant advantages over conventional optical techniques, it should be noted that SMPS-based aerosol metrology in general still possesses some practical limitations. The measurable concentration range is primarily constrained by the counting capacity of the condensation particle counter (CPC) stage, which defines the upper limit of reliable operation. Regarding calibration, while its sizing principle based on electrical mobility is largely insensitive to differences in refractive-index between the calibration particles and target particles [33], the SMPS also requires calibration using monodisperse standard particles such as PSL spheres. Nevertheless, the SMPS-based approach offers significantly higher accuracy and consistency than conventional optical methods, particularly for nanoparticle systems where refractive-index effects and coincidence errors are critical.

Building upon these insights, this research expands aerosol generation and detection techniques by integrating an atomizer and scanning mobility particle sizer (SMPS) and employing a more comprehensive, size-dependent calibration with standard nanoparticles. Specifically, we seek to establish a detailed mapping between liquid-borne particle (hydrosol) concentrations and airborne particle (aerosol) concentrations, in conjunction with correlating particle size information throughout the hydrosol-to-aerosol conversion process. By emphasizing the role of non-volatile residues (NVRs), we aim to illustrate how even trace amounts of surfactants or dissolved solutes can condense into extraneous peaks that must be accurately subtracted from the intended particle distribution.

In pursuing these goals, our work proposes and validates a multi-stage inversion algorithm that (i) measures aerosol particle size distributions (ASDs) with an atomizer-based SMPS, (ii) identifies and subtracts any interfering NVR mode through multi-mode fitting to derive the NVR-subtracted aerosol, and (iii) transforms the "NVR-free" aerosol data into a hydrosol particle size distribution (HPSD) via empirical PSL calibrations. The experimental design encompasses polystyrene latex (PSL) reference particles and CMP slurry samples containing silica and ceria abrasives. By evaluating how different dilution factors (DFs) and solution conditions affect aerosol generation, we confirm the reliability and flexibility of this approach in reconstructing the authentic particle size distributions in liquids.

Regarding equipment optimization and online applicability, the current system maintains a bench-top footprint comparable to other process analyzers and can be readily integrated for inline sampling via direct slurry feed. In practical CMP slurry systems, including storage tanks and point-of-use (POU) pipelines, A-SMPS can be connected directly to the slurry line for real-time monitoring, requiring only the addition of a simple sampling line without any major modification to the existing infrastructure. Even for high-concentration slurries requiring dilution, an inline mixing configuration with a controlled ultrapure-water feed allows immediate concentration adjustment without offline sampling, while the proposed inversion algorithm enables instant recovery of the original slurry concentration and condition for process feedback. This approach supports continuous, representative, and maintenance-free monitoring. Moreover, since the SMPS unit accounts for most of the A-SMPS system volume, ongoing advances in miniaturized DMA and compact CPC designs indicate strong prospects for overall system miniaturization and optimization toward a more efficient monitoring platform [34,35].

Ultimately, the study establishes a practical measurement framework for hydrosol applications that overcomes the limitations of both conventional liquid-phase light scattering methods (e.g., LPC, DLS) and recent industrial online monitoring systems (e.g., at-line DLS and SPOS), thereby offering broader prospects for precision liquid-borne nanoparticle characterization and real-time CMP slurry monitoring.

2. Research Gaps

- Existing aerosol-based measurement studies have primarily focused on aerosol-phase particle characterization, without the ability to quantitatively retrieve liquid-borne (hydrosol) particle concentrations in CMP slurries.
- Previous attempts to correlate aerosol and hydrosol data using single-size volume standards failed to consider the size-dependent relationship between the two phases, limiting their applicability to polydisperse and multimodal slurries.
- While the electrospray-SMPS (ES-SMPS) technique effectively reduces NVR interference, its dependence on high-voltage stability and electrolyte doping hinders continuous, inline industrial use.
- Conventional optical techniques (LPC, DLS) still suffer from refractive-index dependence, coincidence errors, and poor sensitivity below 20–30 nm, making them inadequate for precise CMP slurry characterization.

3. Contributions of this study

- Proposes a compact atomizer–SMPS (A-SMPS) configuration that operates with native CMP slurries without chemical modification, offering a robust and industrially compatible aerosolization platform.
- Develops a multi-stage inversion algorithm that integrates NVR removal and size-dependent aerosol-to-hydrosol mapping, enabling accurate reconstruction of the true particle-only distribution.
- Establishes a quantitative inversion framework combining PSL calibration (for size correlation) and DF correction (for concentration recovery), allowing precise determination of liquid-phase particle concentration solely from aerosol measurements.
- Demonstrates that the proposed system achieves high reliability and accuracy in CMP slurry metrology, bridging aerosol-based

techniques with practical hydrosol characterization for semiconductor process control.

4. Outline of the paper

The remainder of this paper is structured as follows.

Section 5 describes the experimental setup (A-SMPS configuration, materials, and conditions).

Section 6 presents the data-processing framework and multi-stage inversion algorithm and discusses experimental results (PSL calibration, CMP slurry analysis, and long-term stability).

Section 7 concludes the paper.

5. Methodology

5.1. Preparation of hydrosol samples

This study aims to measure the NVR-subtracted hydrosol particle size distribution (HPSD) of nanoparticles by measuring aerosol particle size distribution (ASD) with aerosol metrology. We measured standard nanoparticle Polystyrene Latex nanospheres (PSL) and three CMP slurry samples (one Ceria (CeO_2) and two Silica (SiO_2)). As the measurement setup utilized aerosol metrology with atomizer and SMPS, calibration for measured ASD to HPSD inversion was conducted with standard nanoparticles.

For calibration, we measured PSL (Thermo Fisher Scientific, MA, USA) with five sizes of 50, 100, 200, 500 and 700 nm with various hydrosol concentrations after dilution. As the manufacturer certifies particle size and concentration for each PSL sample, number concentrations were calculated from density and mean diameter. As the size range of the utilized SMPS with long-DMA is approximately 10 to 1000 nm, the particle size of PSL NPs was chosen to cover the overall range of measurement. Since the number concentration of each sample varied based on its particle sizes, the original sample was diluted with ultra-pure water to achieve the number concentration ranged from 1.0×10^8 ml^{-1} to 1.0×10^{11} ml^{-1} for 50, 100 and 200 nm samples and 6.4×10^6 ml^{-1} to 6.4×10^9 ml^{-1} for 500 and 700 nm samples. The diluted number concentration range for 500 and 700 nm samples were set to be relatively lower than the smaller sizes as the number concentration of original samples is lower due to the large volume of larger size samples.

As for the slurry measurements, three types of CMP slurries containing different abrasive particles—one ceria-based (CeO_2) and two silica-based (SiO_2) formulations, hereafter referred to as Ceria Slurry, Silica Slurry, and Silica Slurry 2—were analyzed. The samples are provided by different anonymous manufacturers for proprietary reasons. In the context of chemical mechanical polishing (CMP) for semiconductor fabrication, the abrasive particle size for slurries has decreased to 100 nm, reflecting the miniaturization of the CMP process in comparison to the conventional process and the removal of particles at the microscale. As the exact particle size and concentration information of the slurry samples were blinded, dilution factor was optimized with preliminary test with assumed weight concentration and size for abrasive, and the slurry measurement was conducted with optimized dilution factor range. Moreover, all three slurries are actual process-grade CMP formulations supplied for industrial use rather than simplified laboratory samples.

Each slurry inherently contains multiple surfactants, chemical additives, and pH-control agents that are optimized for specific CMP process conditions. Although the exact formulations are proprietary and undisclosed by the manufacturers, these slurries accurately represent the chemical and compositional complexity typically encountered in real semiconductor manufacturing environments. Summarized information for test samples including material, nominal size and concentration is provided in Table 1.

5.2. Aerosol generation and non-volatile residue formation

To utilize aerosol detection method for hydrosol concentration evaluation, the hydrosol samples must be aerosolized with an aerosol generator. The constant output atomizer (Model 3076, TSI, MN, USA) was utilized as the aerosol generator for this study. For sample injection, the liquid sample solutions with colloid NPs (i.e., hydrosol samples) are directly injected into the atomizer block with a flow rate of ~ 150 μl/min operated under a compressed dry air (CDA) pressure of 30 psi. The expansion of compressed, dried air through an orifice produces a high-speed jet that entrains liquid via a vertical passage into the atomizing region, where it is fragmented into fine droplets. An impactor on the wall opposite the jet removes larger droplets, and surplus liquid is discharged from the base of the atomizer assembly. The aerosol stream, carrying nanoparticles suspended in the liquid, then passes through a silica gel diffusion dryer, which removes the remaining moisture by evaporation. During this process, the water droplets surrounding the particles are evaporated, and the aerosolized nanoparticles are generated by the atomization process as shown in Fig. 1a.

To ensure consistent performance and minimize contamination, a routine maintenance protocol was applied throughout all experiments in this study. The atomizer was flushed with ultra-pure water twice a week, and the silica gel in the diffusion dryer was also replaced twice a week to prevent residue buildup from slurry operation and to avoid moisture saturation that could reduce drying efficiency. These preventive measures were found sufficient to maintain stable aerosol generation and measurement consistency across both short-term and long-term experiments.

Liquid solutions contain chemical additives such as surfactants, which are chemical components such as cationic polymers and anionic polymers that prevent particle agglomeration in the liquid phase [16,36]. When empty droplets only containing non-volatile solutes without native solid particles shrink until complete evaporation, these surfactants condense to form non-volatile residues (NVRs) [16,37]. If the aerosolized particulate population is dominated by NVR rather than target solid particles due to the inappropriate dilution factor, these formed NVR particle peaks can overlap and interfere with the target particle peaks as illustrated in Fig. 1b. Furthermore, if the droplets generated by the atomizer are excessively large and contain large

Table 1
Summarized sample information including sample name, particle material, nominal size, concentration, prepared hydrosol concentration range and sample dilution factor for measurement.

Sample	Material	Nominal size [nm]	Concentration [wt%]	Prepared hydrosol concentration [ml^{-1}]	Sample dilution factor [-]
3050A	PSL	50	1	1.0×10^8-1.0×10^{11}	
3100A	PSL	100			–
3200A	PSL	200			
3500A	PSL	500	1	6.4×10^6-6.4×10^9	–
3700A	PSL	700			
Silica Slurry	SiO_2	~150*	20	–	500, 1000, 2500
Ceria Slurry	CeO_2	~140*	6		250, 500, 1000
Silica Slurry 2	SiO_2	~100*	–		Gradually decreased to 804

* Nominal sizes given by manufacturers.

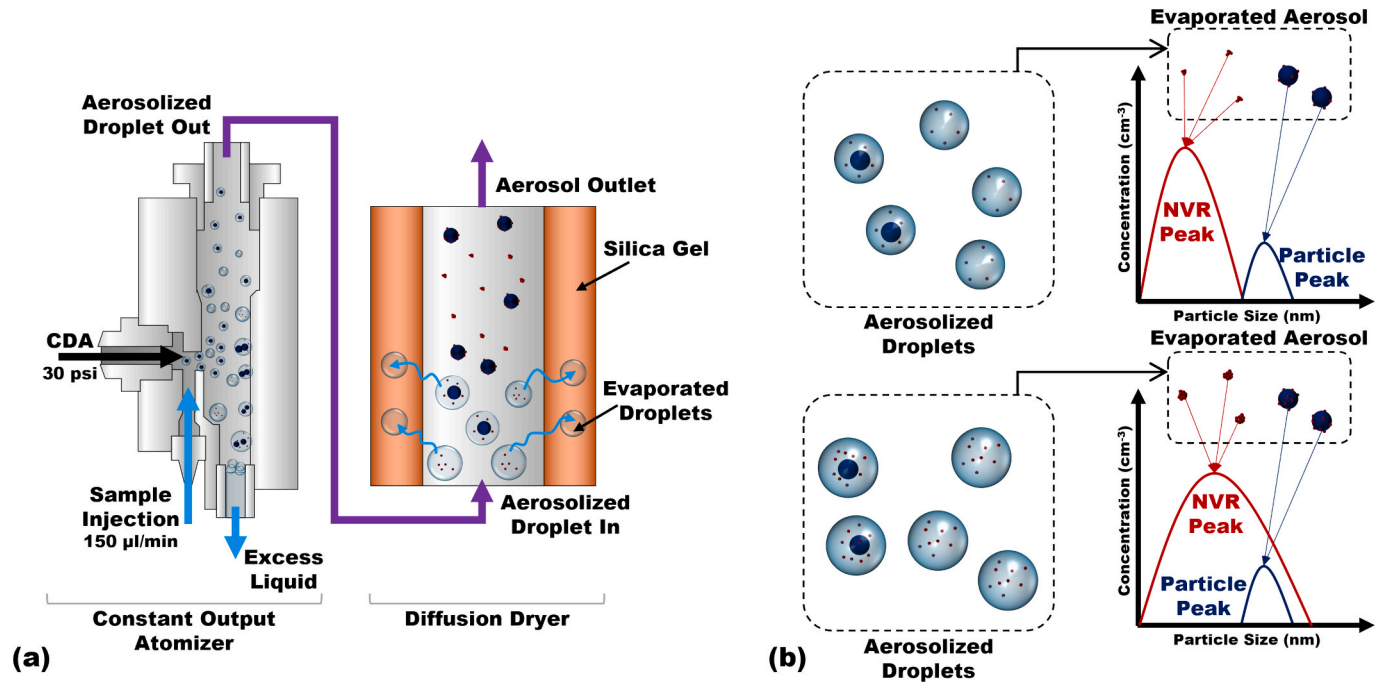

Fig. 1. Schematic diagram explaining (a) aerosol generation process and (b) formation of non-volatile residue from surfactants during droplet evaporation and example of the overlapped NVR and particle peak.

amount of surfactant, this leads to the formation of correspondingly larger NVRs and it can consequently affect the results. To minimize the interference of NVRs, the impaction occurs during the aerosol generation process to remove large droplets. Moreover, optimization of dilution factor of sample plays an important role in separating NVR and particle peaks.

5.3. *Aerosol detection with scanning mobility particle sizer*

Fig. 2a illustrates the experimental setup for this study. After testing samples are prepared and diluted, they are injected into the atomizer. The atomizer block and diffusion dryer are vertically assembled to minimize the particle loss during aerosolization. After the target liquid samples are atomized and evaporation yields aerosol particles, they are subsequently classified and counted by a combination of differential mobility analyzer (DMA) and condensation particle counter (CPC) with bipolar charging by soft X-ray performed prior to measurement as shown in Fig. 2b. As for this combination for measurement, we employed SMPS consisting of an electrostatic classifier (Model 3082, TSI, MN, USA), DMA (Model 3081, TSI, MN, USA) and a butanol-CPC (Model 3075, TSI, MN, USA). This atomizer-SMPS configuration is hereafter referred to as A-SMPS.

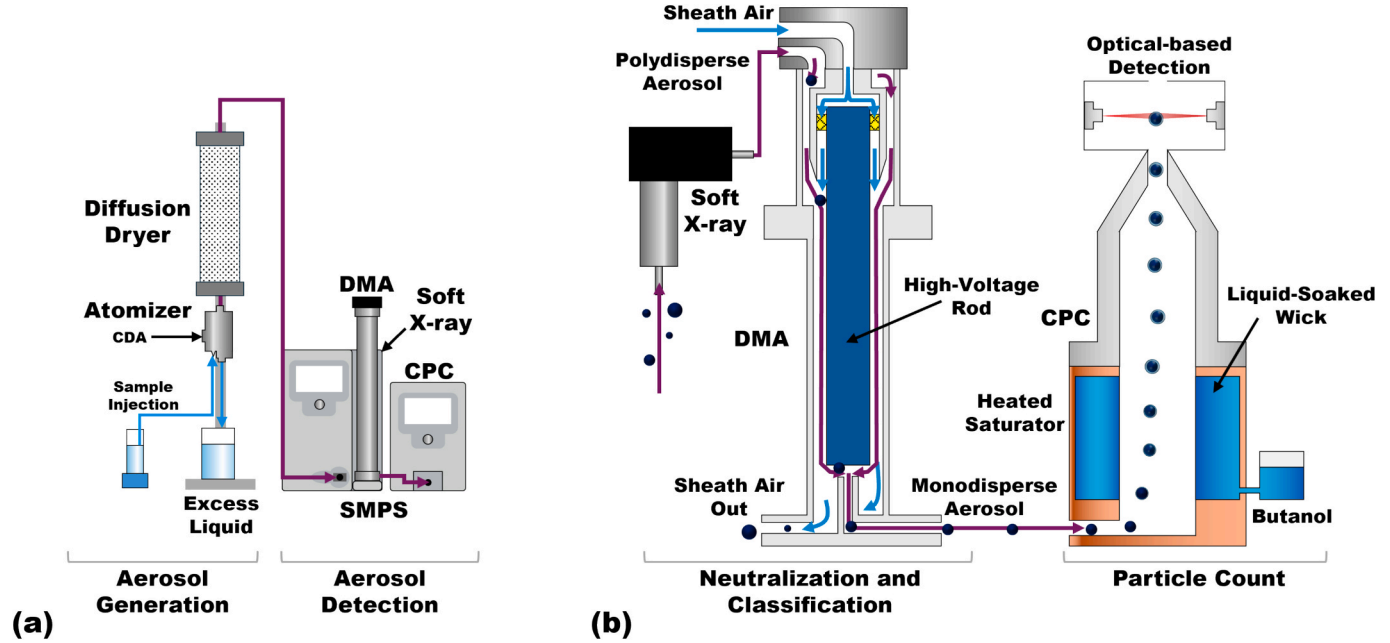

Fig. 2. Schematic diagram of (a) experimental setup and (b) basic mechanism of particle classification based on electrical mobility and particle counting with SMPS (DMA + CPC).

The A-SMPS aerosolizes the hydrosols within liquid solutions and measures aerosol concentration. The atomizer has advantages over the electrospray aerosol generator (EAG) due to its conventional sample injection method and its ability to deliver target particles in-line. Previous studies, however, have shown that EAG generates smaller droplets, producing smaller undesired NVR particle peaks, which makes it easier to distinguish NP peaks from NVR particle peaks [16,26,27]. Despite this advantage of EAG, EAG requires an additional step of mixing a certain amount of ammonium acetate into the sample to adjust electrical conductivity, and it is also challenging to maintain a stable

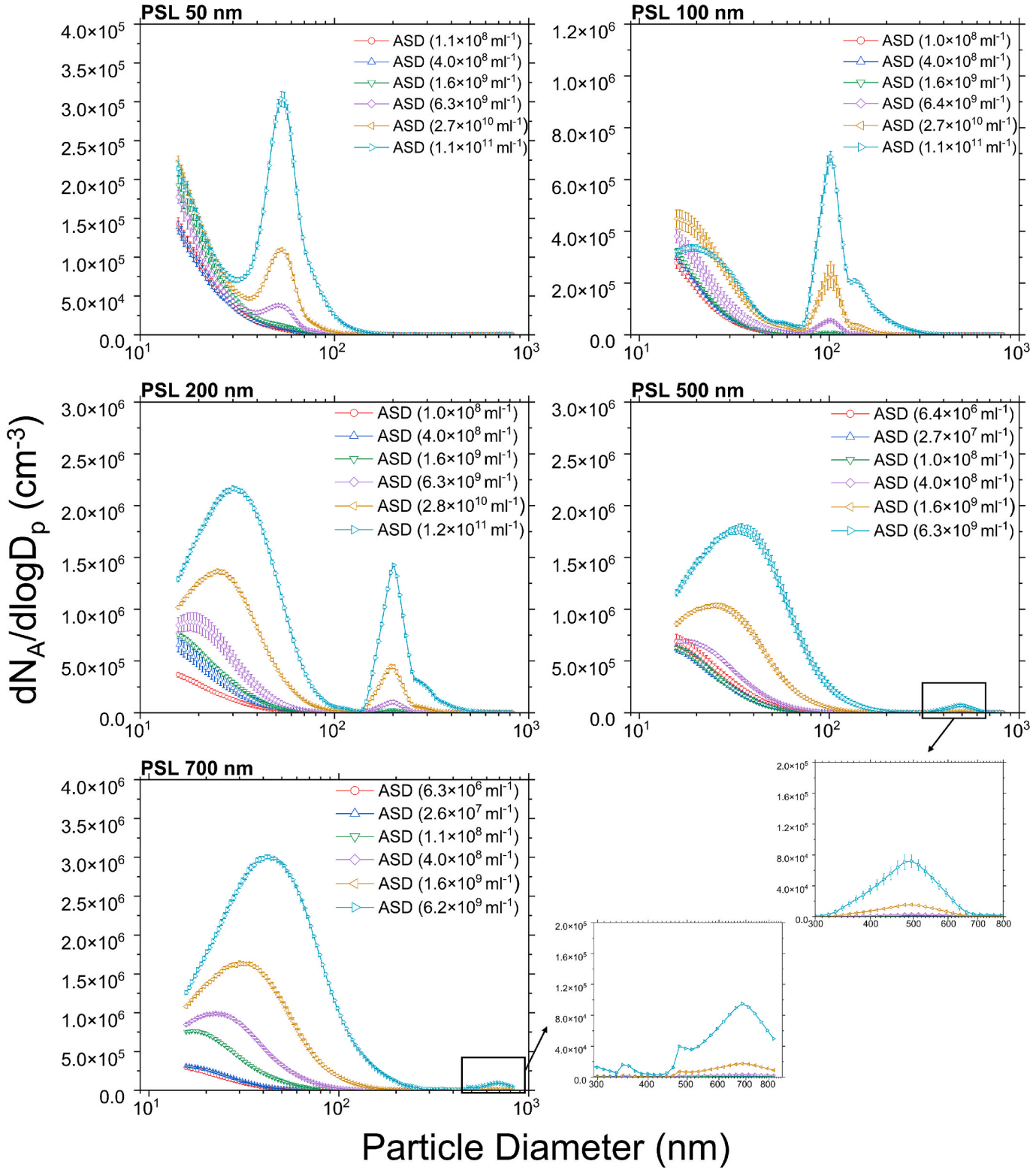

Fig. 3. SMPS-measured aerosol particle size distribution (ASD) results of monodisperse PSL NPs with 50 nm, 100 nm, 200 nm, 500 nm and 700 nm of particle sizes measured by A-SMPS. The concentration information in parentheses represents number concentrations of each diluted sample, calculated from the manufacturer-specified stock concentration.

Taylor cone mode over extended periods [26,28,38]. Therefore, for semiconductor process monitoring—specifically CMP slurry monitoring—where ease of use and stable, long-term sample delivery are critical, the atomizer offers clear benefits. For these reasons, this study employed the atomizer instead of the EAG. After generation of aerosols, particles are first charge-neutralized by a soft X-ray neutralizer and then enter DMA, where the aerosol and sheath flows are regulated and an electric field is applied for size-based particle classification of the monodisperse particles throughout the polydisperse particles. The classified monodisperse particles are subsequently counted by the condensation particle counter (CPC). The scanning time was set to be 180 s to extend the measurable particle size range, and the aerosol and sheath flow rates in DMA were set to be 1.0 and 2.5 L/min, respectively.

6. Results and Discussion

6.1. PSL measurements

To carry out the calibration by monodisperse PSL characterization, each original sample was serially diluted to six discrete hydrosol number concentration levels and the measurements were carried out sequentially following concentration order, from the lowest to the highest level. As previously stated, the aerosolization process typically resulted in the formation of residual particles, comprising the evaporation of non-volatile solutes from the blank droplets devoid of main particles. The experimental results for monodisperse PSL measurement illustrated in Fig. 3 indicate that as particle size decreases, peak overlap with the NVR mode becomes more likely, degrading size distribution accuracy. The results also establish a positive correlation between PSL particle size and resultant NVR mode diameter as shown in Fig. 3. This trend suggests that larger PSL spheres contain higher surfactant levels to mitigate aggregation, shifting the NVR mode accordingly [30].

The lower detection limit of hydrosol concentration for each sample has also been evaluated by comparing the measured concentration of samples within range of particle mode obtained by higher concentration samples to that of ultra-pure water measurement with same size range. As for the 50 nm PSL, the concentration under 4.0×10^8 ml^{-1} showed unreliable data and uncertain particle mode as the residue peak overwhelmed the particle peaks. This slight oversizing of the 50 nm PSL peak originates from non-volatile residues (NVRs) that remain after droplet evaporation, an effect well documented in aerosol-based nanoparticle metrology [16,18]. When the generated droplets are comparable in size to or larger than the particle core, even trace amounts of surfactant or solute condense into residual shells, artificially increasing the apparent mobility diameter measured by SMPS. Consequently, such residue-induced broadening and peak shift define the practical lower detection limit of the present A-SMPS configuration, which is approximately 50 nm under the tested conditions. Measurements below this range are increasingly dominated by NVR artifacts rather than true particle signals, making accurate size extraction unreliable. As the large particles with 500 and 700 nm PSL had lower concentration range for measurement compared to the other sizes, they both showed comparatively lower level of distribution compared to the smaller sizes of PSL and even to the NVR peak of themselves, and they both showed 4.0×10^8 ml^{-1} as a lower detection limit. Consequently, the dilution factor and concentration optimization are crucial for accurately defining the size distribution for target particles.

6.2. Data process for ASD to HPSD inversion

While adapting aerosol metrology for measuring hydrosol samples validated its reliability and feasibility, it still requires an essential step in converting SMPS measured ASD into the corresponding HPSD. Since standard nanoparticles such as PSL and gold nanoparticles (Au NPs) are commonly employed for calibration purposes, they not only possess certified particle sizes with geometric mean diameter and geometric standard deviation but also provide comparatively precise hydrosol concentration data. Consequently, even an SMPS-based ASD analysis alone can yield valuable information regarding the hydrosol particle size distribution. However, for most hydrosols used in various application fields such as semiconductor manufacturing processes, their exact particle sizes and hydrosol concentrations are not well-established. As a result, even if one performs an ASD measurement using an optimized recipe, it becomes difficult to quantitatively analyze the original HPSD for its intended purpose.

Accordingly, the PSL data acquired in the preliminary stage were used to quantify the correlation between APSDs and HPSDs. Leveraging this empirical relationship, we devised an algorithm that converts the SMPS–measured ASD of a hydrosol sample with various sizes into its corresponding HPSD.

The size distribution measured by SMPS can be expressed as $dN_A/d\log_{10}D_p$. To quantitatively obtain the correlation between aerosol number concentration N_A and prepared hydrosol number concentration N_H of PSL, the NVR-subtracted aerosol particle number concentration $N_{A,\ PSL}$ should be obtained by priority.

In our approach to PSL-based calibration, a bimodal lognormal fitting step is applied first following the equation:

$$\frac{dN_A}{d\log_{10}D_p}(D_{p,i}) = A_1\exp\left[-\frac{1}{2}\left(\frac{lnD_p - ln\mu_1}{\sigma_1}\right)^2\right]_{NVR} + A_2\exp\left[-\frac{1}{2}\left(\frac{lnD_p - ln\mu_2}{\sigma_2}\right)^2\right]_{PSL} \quad (1)$$

where A is mode amplitude, μ is geometric mean diameter, σ is geometric standard deviation of each log-normal mode. The fitted results for each sample showed R-squared value over 0.99 and confirmed its reliability.

By integrating the separated PSL ASD as follows:

$$N_{A,PSL} = \int A_2\exp\left[-\frac{1}{2}\left(\frac{\ln D_p - \ln\mu_2}{\sigma_2}\right)^2\right]_{PSL} d(\ln D_p) \quad (2)$$

we obtained the NVR-subtracted aerosol particle number concentration N_{AP} of PSL (i.e., $N_{A,\ PSL}$).

The obtained $N_{A,\ PSL}$ is then compared against the corresponding N_H, which is already known from certified data. By comparing them with a linear regression for various particle diameters d_{PSL} by following equation:

$$\log_{10}(N_{A,PSL}) = A(d_{PSL}) \times \log_{10}(N_{HP}) + B(d_{PSL}) \quad (3a)$$

each sample showed the correlation as shown in Fig. 4a. As illustrated in Fig. 4b, the fitted coefficients $A(d_{PSL})$ and $B(d_{PSL})$ in Fig. 4b exhibit clear monotonic dependences on particle diameter, with high coefficients of determination ($R^2 = 0.992$ and 0.977, respectively). This trend indicates that particle transmission from the hydrosol to aerosol phase is size dependent. Accordingly, the present inversion procedure employs these size-resolved coefficients to reconstruct the NVR-subtracted hydrosol distribution, thereby compensating for such losses. One of the previous studies highlighting the aerosol metrology for hydrosol measurement utilized a single-size volume standard to correlate aerosol and hydrosol concentrations [16]. Our approach extends that framework by establishing an explicit size-dependent mapping, ensuring accurate conversion across a wide particle-size range.

Based on the obtained relationship, an APSD-to-HPSD inversion formula can be established for each particle size as follows:

$$\log_{10}(N_{AP}) = A\left(\mu_{rep}\right) \times \log_{10}(N_{HP}) + B\left(\mu_{rep}\right) \quad (3b)$$

where μ_{rep} is the particle representative mean diameter.

Through this procedure, it ensures that the subsequent correlation and inversion steps focus solely on the intended particle population,

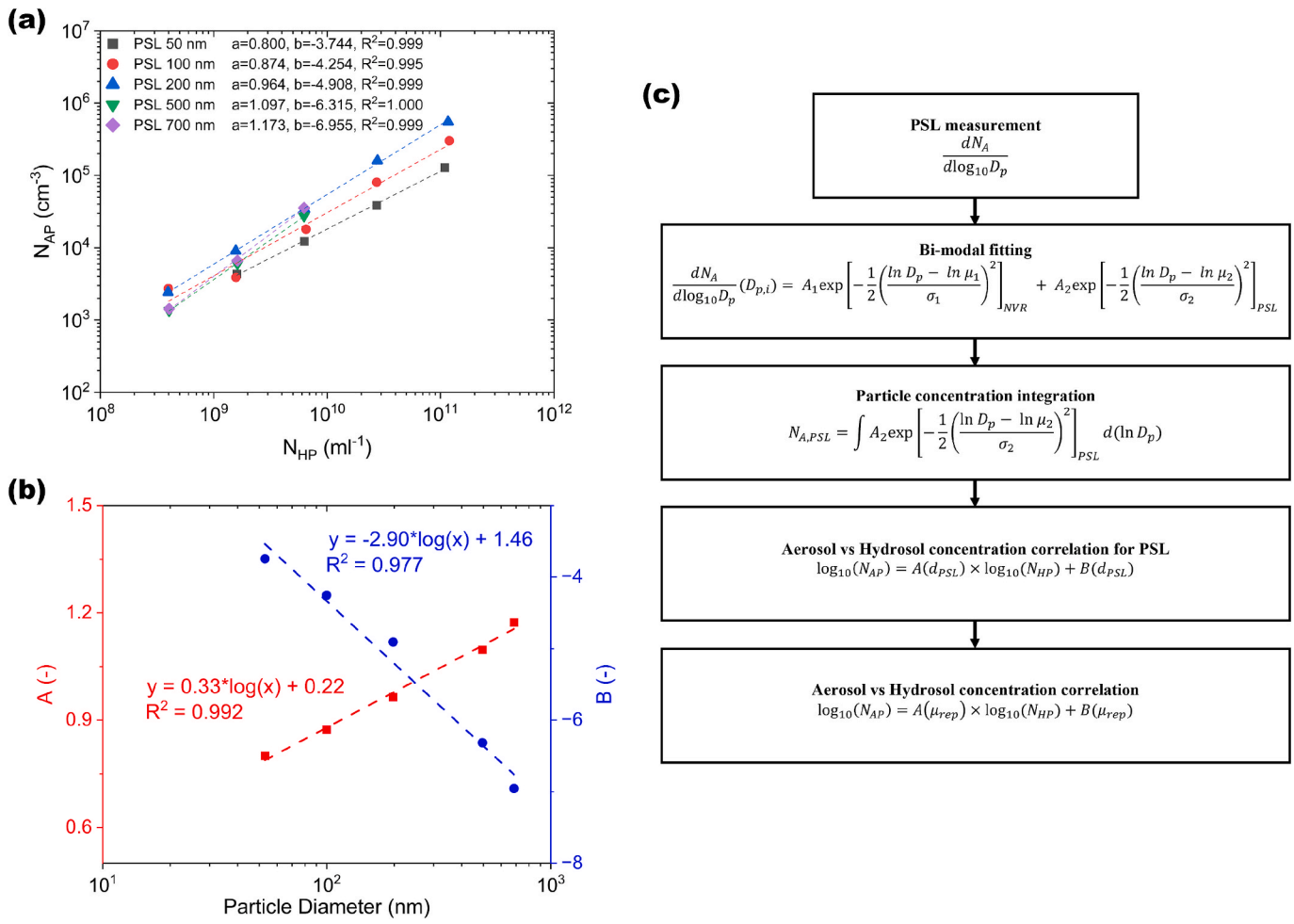

Fig. 4. (a) Lognormal linear regression of NVR-subtracted aerosol particle number concentration N_{AP} obtained by bi-modal fitting of aerosol size distributions versus NVR-subtracted hydrosol number concentration N_{HP} for various PSL sizes, (b) the resulting coefficient A and B for N_{HP} and N_{AP} correlation as functions of particle mean diameter, and (c) summarized flow diagram for obtaining hydrosol and aerosol number concentration correlation.

thereby enhancing the overall reliability and accuracy of the calibration results.

6.3. Algorithm for NVR-subtracted particle size distribution

While a framework for converting APSD to HPSD was established, that inversion depends on isolating the genuine particle signal from any interfering NVR as the inversion function has particle representative mean diameter μ_{rep} as a key parameter. To accomplish this, we integrate a multi-mode SMPS fitting procedure for NVR subtraction with the aerosol to hydrosol inversion logic, ensuring that the aerosol data to be analyzed is NVR-free and having clear mean diameter before being mapped into the hydrosol domain. The outcome is an NVR-subtracted hydrosol particle size distribution (HPSD), which accurately reflects the true particle concentration and size distribution of colloidal nanoparticles in the liquid phase without interference.

This algorithm begins by modeling the raw ASD $dN_A/\mathrm{dlog}_{10}D_p$ acquired by SMPS with multi-modal fitting by

$$F_k(D_{p,i}) = \sum_{j=1}^{k} A_j exp\left[-\frac{1}{2}\left(\frac{ln(D_p) - ln(\mu_j)}{\sigma_j}\right)^2\right]_{k=2..4} \quad (4)$$

where a sum of up to four log-normal components with k indicating the set number of modes for multi-modal fitting, each having amplitude A_j, geometric mean diameter μ_j, and geometric standard deviation σ_j represents the fitted model for raw data.

Following this multi-mode fitting, the residual sum of squares for each mode count k, SSE_k, is calculated as

$$SSE_k = \sum_i \left[y_i - F_k(D_{p,i})\right]^2 \quad (5)$$

and compared to the total variance of the dataset, $SST = \sum_i \left[y_i - \bar{y}\right]^2$.

The coefficient of determination, $R_k^2 = 1 - \frac{SSE_k}{SST}$, quantifies the goodness of fit for each k from 2 to 4. The mode count k maximizing R^2 is then chosen as the best representation of the measured ASD. Here, SSE_k represents the residual error between the measured data and the fitted function F_k, while SST denotes the total variability of the data. A higher R_k^2 indicates a better agreement between the fitted curve and the measured ASD. The mode number k giving the highest R_k^2 is therefore selected as the optimal number of log-normal components, ensuring that the measured distribution is represented accurately without unnecessary overfitting.

Once mode number k is determined, each fitted log-normal mode indexed by j must be classified as either NVR or particle. If k is determined to be 4 and yields two large-diameter modes whose geometric means μ_3 and μ_4 differ by less than 10 % as

$$\frac{|\mu_4 - \mu_3|}{(\mu_4 + \mu_3)/2} < 0.1 \quad (6)$$

the algorithm merges them into a single effective particle mode.

Consequently, those overlapped modes are set as the particle mode as follows:

$$\mu_j\big|_{j=1,2} \Longrightarrow j \in \mathscr{J}_{NVR} \tag{7}$$

, and

$$\mu_j\big|_{j=3,4} \Longrightarrow j \in \mathscr{J}_{Particle} \tag{8}$$

This threshold serves as a practical compromise between numerical variation in fitted parameters and the physical indistinguishability of peaks in that size range. In other words, if μ_3 and μ_4 lie so close that their lognormal curves significantly overlap, treating them as a single peak reduces spurious splitting. From a statistical perspective, this merging step mitigates false positives for mode duplication: an overly strict cutoff risks coalescing genuinely separate peaks, whereas a too-lenient criterion may preserve illusory double modes. Hence, around 10 % acts as a practical boundary reflecting both numerical and physical constraints, particularly typical polydispersity levels in colloidal or aerosol systems [39,40].

In practice, applying the multi-modal fitting to CMP slurry data can produce several adjacent sub-modes in the particle-size region, since the underlying distribution is unknown and affected by NVR overlap. If only the slope-based cutoff and R^2 criterion were used, a single physical mode could be split into multiple fragments, some of which might be misclassified as NVR. To prevent this over-segmentation, a 10 % geometric-mean merging rule is applied: adjacent modes whose geometric-mean diameters differ by less than 10 % are merged before the NVR/particle grouping step. Conceptually, this threshold corresponds to the typical half-width of moderately lognormal CMP peaks (σ_g in the 1.2–1.4 range) for which the FWHM is on the order of ± 10 % of the geometric mean; modes closer than this are therefore treated as a single physical population. With this safeguard, the algorithmic workflow proceeds as follows: (i) multi-modal fitting with $k = 2$ to 4 and selection by R^2; (ii) 10 % merging of adjacent sub-modes; (iii) classification of merged modes into NVR and particle groups; and (iv) construction of the particle-only envelope for inversion, with the NVR envelope treated as an interference to be subtracted. This stepwise scheme yields a particle-only PSD that is resilient to NVR overlap and over-segmentation artifacts, which have historically limited aerosol-based hydrosol metrology. Moreover, leaving these two nearly identical modes separated may induce overfitting, a well-known issue in statistical modeling Overfitting arises when a model uses extra components to capture fluctuations that are random noise or minor numerical artifacts, thus inflating its parameter count without genuinely improving predictive accuracy. Here, retaining two closely spaced peaks can artificially inflate parameter sets in ways that do not reflect distinct physical populations. In conclusion, the 10 % threshold discourages unwarranted complexity.

If no such overlapped modes appear or the mode number k is determined to be less than 4, the algorithm employs a slope-based cutoff to identify whether the fitted curve $F_k(D_{p,i})$ undergoes a negative-to-positive sign change in its local slope with respect to $\log_{10}(D_p)$. Specifically, for each discrete channel i, the slope is approximated by

$$Slope_i = \frac{F_k(D_{p,i+1}) - F_k(D_{p,i})}{log_{10}(D_{p,i+1}) - log_{10}(D_{p,i})} \tag{9}$$

and the algorithm evaluates the specific channel where consecutive slope products result in a sign change, and the algorithm sets the boundary point as $D_{p,\ \mathrm{Cutoff}}$ for distinguishing NVR and particle modes as follows:

$$D_{p,i} = D_{p,Cutoff} \ \text{ if } \ Slope_{i-1} < 0 \ \text{ and } \ Slope_i > 0 \tag{10}$$

.

In other words, a slope transition from negative to positive thus indicates a distinct crest in the distribution and that point is designated as $D_{p,\ Cutoff}$.

All modes satisfying

$$\mu_j < D_{p,Cutoff} \Longrightarrow j \in \mathscr{J}_{NVR} \tag{11}$$

and

$$\mu_j \geq D_{p,Cutoff} \Longrightarrow j \in \mathscr{J}_{Particle} \tag{12}$$

are consequently assigned to NVR or particle index, respectively.

This approach is founded on the principle that genuinely distinct size populations frequently yield local maxima or inflection points in the aggregate distribution. If the slope changes sign from positive to negative, it implies a distinct crest in the multimodal structure, which can serve as a boundary $D_{p,\ Cutoff}$. From a numerical standpoint, slope sign reversals tend to be robust against small parameter fluctuations, thus acting as an objective criterion for segmenting the distribution. By examining slopes in adjacent intervals, the algorithm further mitigates the risk of random noise producing a false boundary.

Fig. 5 depicts the overall process with SMPS measured data of different slurry samples, showcasing (i) the raw data, (ii) multi-mode lognormal fits, and (iii) the final division of modes into NVR and particle categories. The raw data of ceria slurry showed the fitted results with 4 modes and μ_3 *and* μ_4 showed the overlapped modes, they were integrated into single particle mode. On the other hand, fitted results for silica slurry showed 4 distinct modes thus the slope-based cutoff was determined and the NVR and particle modes are separated according to the set boundary.

Once the particle mode index $\mathscr{J}_{Particle}$ is defined, the APSD can be obtained by summing over those modes as

$$\frac{dN_{AP}}{d\log_{10}D_p}(D_{p,i}) = \sum_{j\in\mathscr{J}_{Particle}} A_j \exp\left[-\frac{1}{2}\left(\frac{\ln(D_p) - \ln(\mu_j)}{\sigma_j}\right)^2\right] \tag{13}$$

To convert the refined APSD of test particles into HPSD, the APSD-to-HPSD inversion algorithm obtained based on PSL calibration should be utilized. The particle representative mean diameter μ_{rep} of separated APSD is calculated as

$$\mu_{rep} = \underset{D_p}{argmax}\left(\frac{dN_{AP}}{d\log_{10}D_p}(D_{p,i})\right) \tag{14}$$

where the maximum peak point for the distribution is identified.

The final stage converts this APSD into a HPSD by means of a PSL calibration or an analogous reference equation, combined with any required dilution factor. As the measured sample is typically analyzed in a diluted form, the original solution's hydrosol concentration is recovered by multiplying the measured HPSD values by the sample's dilution factor, thereby yielding the original solution's HPSD (i.e., DF-corrected HPSD) and its corresponding DF-corrected original number concentration, DF × N_{HP}.

$$\frac{dN_{HP}}{d\log_{10}D_p}(D_{p,i}) = 10^{\left(\log_{10}\left(\frac{dN_{AP}}{dlogD_p}(D_{p,i})\right) - B(\mu_{rep})\right) \Big/ A(\mu_{rep})} \times DF \tag{15}$$

Fig. 6 outlines the total algorithmic flow including multi-mode fitting attempting to find the best mode, the assigned or merged modes, and the inversion from APSD to HPSD to carry out the reliable data processing to obtain HPSD by SMPS measurement. By systematically removing the NVR component, the user obtains a more reliable reflection of the actual particle population, ensuring that subsequent hydrosol concentration analyses reflect the main particles rather than including artifacts from extraneous residues.

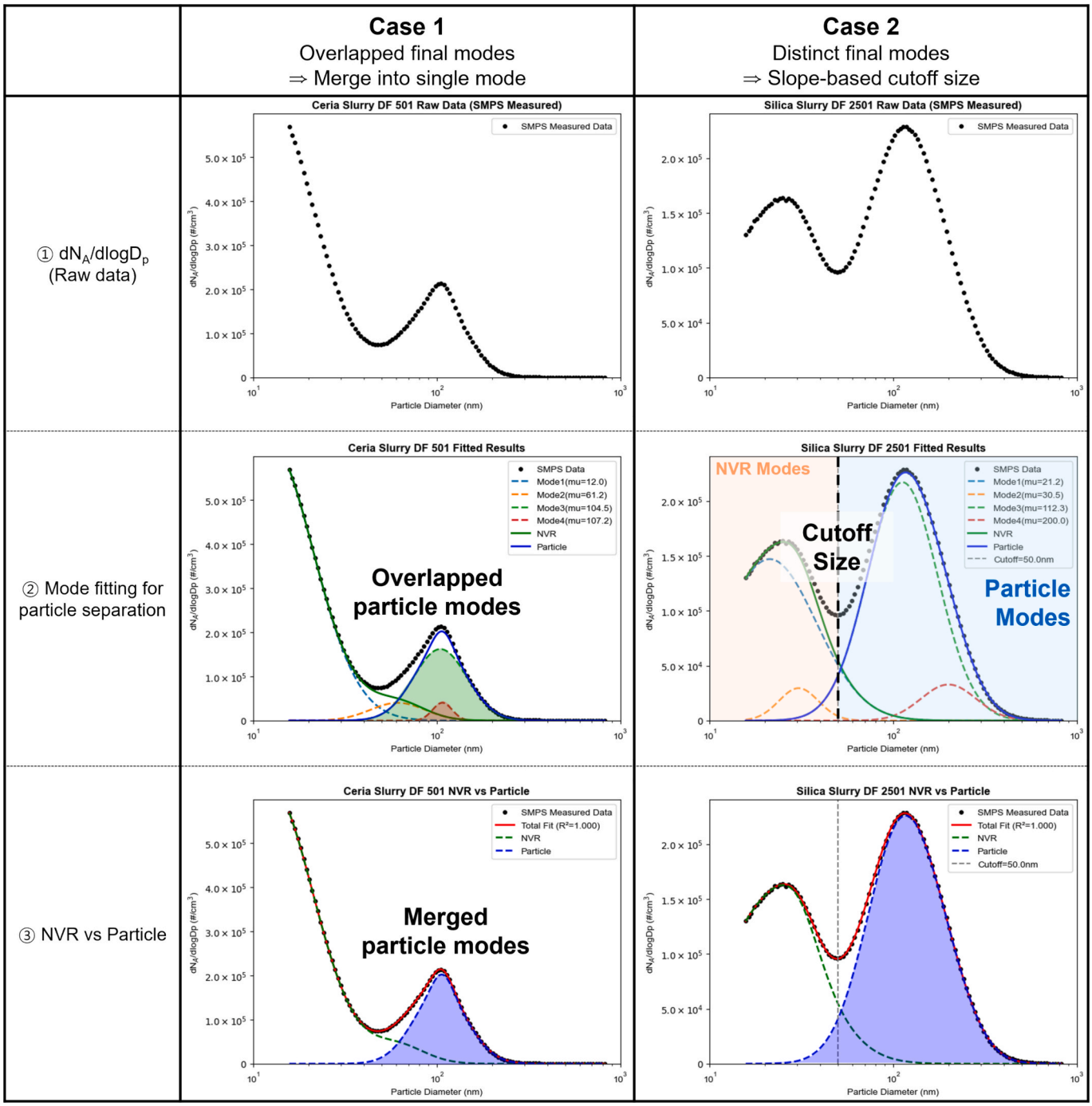

Fig. 5. Illustrative multi-mode lognormal fitting of SMPS measured ASD for distinguishing NVR-subtracted aerosol particle size distribution (APSD) from total ASD: examples of two distinguished cases with potential mode overlaps and slope-based cutoff size determination for APSD analysis.

6.4. *Hydrosol particle size distribution results*

Two types of CMP slurries having abrasive material type of Ceria and Silica were measured by SMPS and the NVR-subtracted hydrosol particle size distribution (HPSD) obtained from the multi-step data processing was examined. Each sample was measured with varying DFs. The experimental design involved selecting an appropriate DF range based on nominal size and weight concentration information, aiming to get clear particle peak with SMPS measurements. In practice, neither ceria nor silica slurries required additional parameter tuning and the initial DFs sufficed to produce distinct particle peaks within the ASD. After applying the processing algorithm, each slurry's APSD was converted into the DF-corrected HPSD.

Fig. 7 contrasts the raw SMPS ASDs measured in 20 scans and the processed DF-corrected HPSDs for three different DFs in (a) ceria and (b) silica slurries. The graph illustrating the separation of NVR and particle modes using multi-mode lognormal fitting is presented in Fig. S1. In both cases, the raw ASD reveals a prominent non-volatile residue (NVR) mode at smaller diameters. Nonetheless, a particle-mode region remains visible, especially in the higher-concentration samples (i.e., lower DF), where the measured count tends to increase. Fig. 7a illustrates that all three DF samples yield nearly identical DF-corrected HPSDs, demonstrating the consistency of the DF correction: once the NVR mode is subtracted, the main particle mode matches closely across different

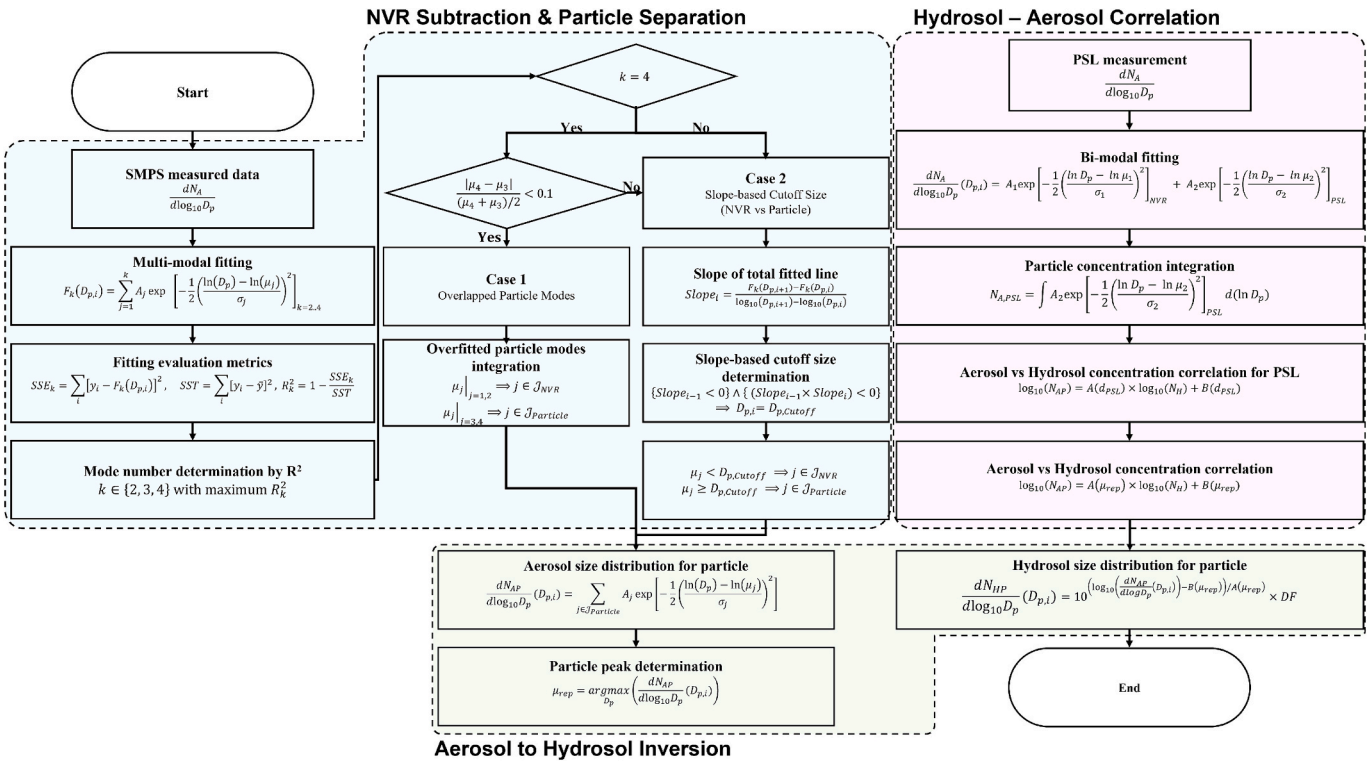

Fig. 6. Flow diagram for obtaining an NVR-subtracted particle size distribution, encompassing multi-mode fitting, NVR isolation with mode assignment, and ultimate hydrosol conversion steps.

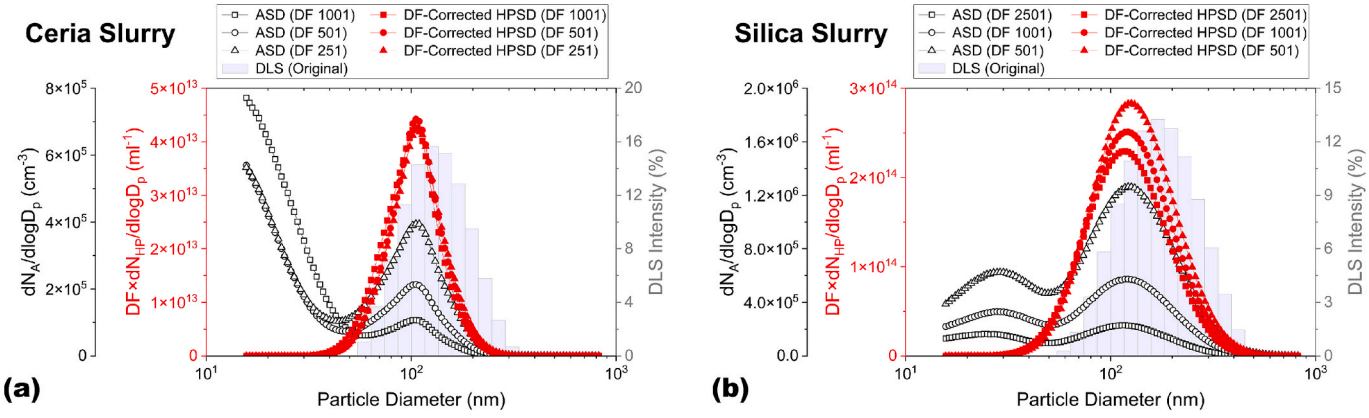

Fig. 7. SMPS-measured aerosol particle size distributions (ASDs) including NVRs and processed DF-corrected NVR-subtracted hydrosol particle size distributions (DF-corrected HPSDs), alongside DLS intensity measurements for (a) ceria slurry and (b) silica slurry at three different dilution factors (1001, 501 and 251 for Ceria; 2501, 1001 and 501 for Silica).

levels of dilution. This near overlap suggests that the original (undiluted) colloidal suspension is effectively reconstructed, supporting the reliability of the approach.

In the silica slurry data depicted in Fig. 7b, the DF-corrected HPSD curves likewise exhibit comparable mean diameters among the three tested DFs, but with increasing concentration, the results show a slight shift of the mean diameter and increasing amplitude. Such behavior may reflect minor interactions among suspended particles, a mild increase in polydispersity under more concentrated conditions, or small systematic biases in the nebulization and detection processes. Importantly, the approach still yields a coherent peak consistent with the expected particle size range, confirming the method's flexibility even when minor distribution shifts occur.

DLS measurement results of undiluted slurry samples indicate the intensity-weighted peaks at particle diameters larger than the SMPS-based DF-corrected HPSD. This outcome accords with the known disproportionate scattering contribution from larger particles in DLS, commonly shifting the peak to higher diameters. Despite that offset, the DLS data validates that both ceria and silica samples maintain their primary particle population in the size range the SMPS algorithm identifies once NVR is removed.

Fig. 8 compares the hydrosol particle number concentration N_{HP} among different DFs and shows how DF-corrected original number concentration (DF × N_{HP}) approximate the original (undiluted) concentration. To provide an explicit quantitative assessment, two complementary metrics were adopted: (i) the mean and coefficient of variation (CV) of DF × N_{HP} across the tested DFs, which evaluates whether DF correction conserves the original concentration; and (ii) the coefficient of determination R^2 from a linear regression of N_{HP} versus the fractional concentration 1/DF, which tests the expected proportionality

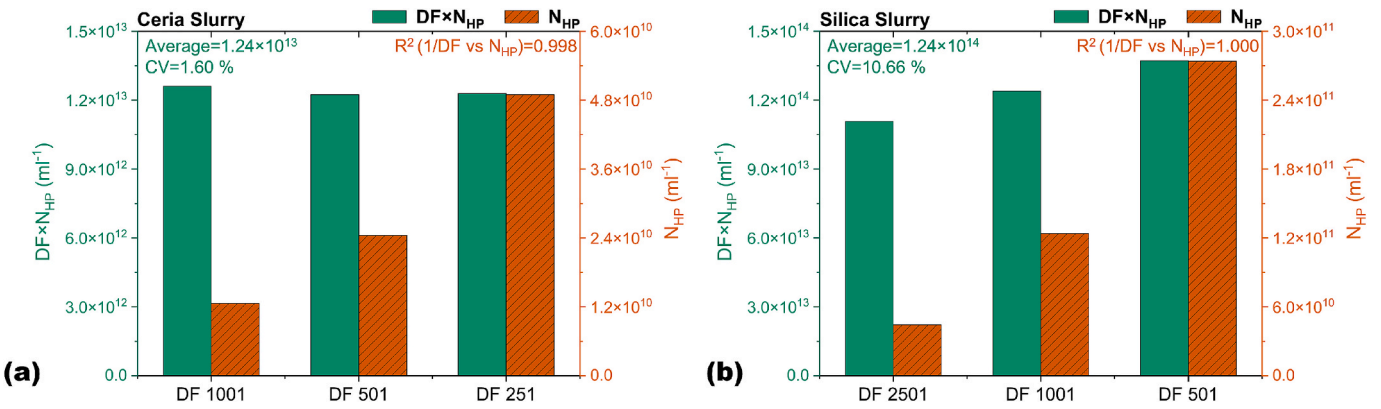

Fig. 8. Hydrosol particle number concentration N_{HP} of diluted samples and DF-corrected original number concentration (DF × N_{HP}) of (a) ceria slurry and (b) silica slurry.

of the measured number concentration to dilution. For ceria slurry, the DF × N_{HP} closely coincide with all three DFs, indicating that the undiluted original sample concentration can be accurately obtained by diluted samples within optimized range. Consistently, DF × N_{HP} exhibits a low CV and the N_{HP}-1/DF regression yields R^2 close to unity, quantitatively confirming both concentration conservation after DF correction and linear scaling with dilution. As for the silica slurry, the result reveals an insignificant upward trend as the sample concentration increases (i.e., DF decreases). Even so, DF × N_{HP} remains nearly constant within a modest CV, and the N_{HP}-1/DF relationship maintains a near-unity R^2. The N_{HP}-1/DF correlation graph of both samples are shown in Fig. S2.

Despite the overall high accuracy and reliability demonstrated by the data, Silica slurry results in Fig. 7b and Fig. 8b shows that both the DF-corrected HPSD (DF × $dN_{HP}/d\log_{10}D_p$) and the DF-corrected original number concentration (DF × N_{HP}) exhibit a slight elevation at lower DF (i.e., higher concentration). In the PSD, this manifests primarily as an intensified right-hand shoulder (an elevated distribution envelope rather than a shift of the mode), while in the concentration domain it appears as a small positive bias in DF × N_{HP} across dilutions. We interpret the inter-DF spread (CV = 10.66 %) as an empirical, conservative uncertainty bound for recovering the original number concentration under silica-like matrices, since it aggregates concentration-dependent aerosolization physics (e.g., droplet occupancy and multiplet statistics), subtle changes in atomization efficiency, and small residuals in NVR subtraction. Likewise, the point-wise envelope formed by the DF-corrected HPSDs provides a practical uncertainty band for the size distribution: the mode diameter remains stable within only a few nanometers, whereas the amplitude varies within the inter-DF envelope defined by Fig. 7b. Importantly, as shown in the long-term test in Section 6.5, once DF is held constant the scan-to-scan variability collapses to only a few percent with no observable drift, indicating that the inter-DF effect is best regarded as a systematic, concentration-regime component, while the repeatability of the measurement system and the algorithm at fixed DF is substantially better. Accordingly, for practical reporting we distinguish between inter-DF systematic effects and within-DF repeatability.

In summary, these results confirm that the DF-corrected HPSD remains consistent across multiple samples and DFs, reinforcing the integrity of the DF correction. The method effectively captures the particle-size characteristics of the CMP slurries without interference from NVR, and the small shifts observed at higher concentrations are consistent with expected colloidal behavior.

Overall, these findings demonstrate that the algorithm involving aerosol-based particle size measurement, NVR subtraction, and hydrosol inversion with DF correction consistently yields a coherent hydrosol particle size distribution for CMP slurries under various dilution settings. Despite minor shifts in distribution and total concentrations of silica slurry, the near overlap of DF-corrected HPSDs across multiple DFs confirms that the processed distributions align closely with each sample's undiluted state. Taken together, these results not only underscore the reliability of the data-processing framework in isolating the genuine particle mode from NVR interference, but also illustrate how a systematic dilution strategy, guided by nominal particle size and weight concentration, can generate well-resolved DF-corrected HPSDs. Thus, the approach promises broad applicability for precise hydrosol characterization, offering a flexible yet rigorous means to reconcile aerosol-phase measurements with the actual hydrosol properties required for process optimization and fundamental slurry analysis.

6.5. *Long-term data stability evaluation with constant-flow-rate slurry injection*

In practical CMP processes, slurry flow typically involves continuous recirculation and extended operational periods; therefore, ensuring long-term monitoring stability is a critical requirement. To validate the performance of the measurement system and algorithm under prolonged operation, a 48-hour continuous test was conducted using a silica-based CMP slurry sample, referred to as Silica Slurry 2. This experiment was designed to mimic realistic CMP conditions with constant-flow slurry delivery, thereby extending our validation beyond the two slurry tests and demonstrating the algorithm's generalizability over prolonged operation.

As shown in Fig. 9a, a large-volume slurry-circulation system was constructed for the long-term test. Approximately 18 L of ultra-pure water was first charged to a reservoir, and Silica Slurry 2 was injected into the tank at a constant flow rate of 160 μL/min. To continuously mix the slurry and suppress particle settling, a magnetic-levitation pump (Model BPS-iF100, Levitronix, Zurich, Switzerland) was employed; its bearingless, contact-free impeller minimizes wear and virtually eliminates particle shedding during long-term recirculation. In contrast to diaphragm pumps, which generate pulsating flow and pressure via reciprocating membranes and check valves (often necessitating pulsation dampers), the magnetic-levitation pump delivers smooth, electronically controlled flow that reduces shear and cavitation hot spots that can promote slurry agglomeration and CMP defects. Additionally, a laboratory water bath (Model DCWB05, LK Labkorea, Namyangju, Republic of Korea) maintained a constant slurry temperature to reduce thermal drift, thereby minimizing temperature-induced agglomeration in silica-based CMP slurries [41].

The test was divided into two phases: Phase I (0 to 24 h) for slurry injection with constant flow rate, and Phase II (24 to 48 h) where injection was halted but circulation continued. Throughout both phases, the A-SMPS continuously measured the evolving aerosol size distributions of sampled circulating slurry. The scanning time for each SMPS

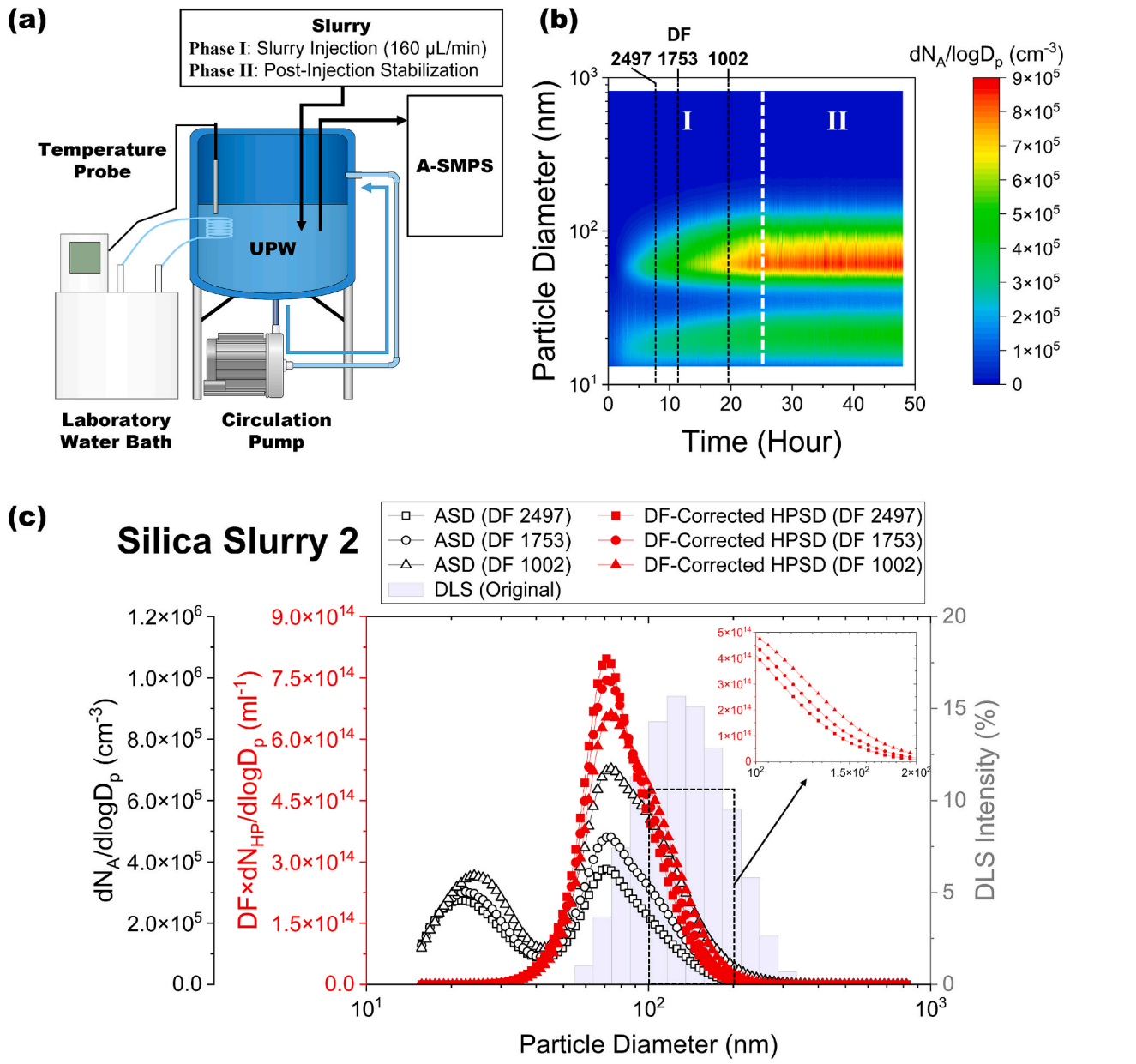

Fig. 9. Long-term stability evaluation under continuous slurry injection and post-injection stabilization: (a) schematic of the experimental setup for long-term measurement with a recirculating tank initially filled with ultra-pure water and continuously injected with slurry; (b) time-resolved $dN_A/d\log_{10}D_p$ contour showing particle concentration evolution across long-term measurement; (c) comparison of SMPS-measured ASDs, DF-corrected HPSDs, and DLS intensity distribution at the three representative DF points indicated in (b) (2457, 1753 and 1002).

measurement was set to 180 s, and a total of approximately 940 scans were conducted over the 48-hour period. Fig. 9b presents a time-resolved contour of the SMPS-measured ASD over the 48-hour period. During Phase I, as slurry was continuously added with constant flow rate, the overall particle concentration in the tank increased steadily. This is seen in Fig. 9b as a growing intensity of the main particle-mode band over time, while the small-diameter NVR mode remained present but distinguishable. By the end of Phase I (at ~ 24 h), the slurry had reached a dilution factor of around 804. At that point the injection was stopped, marking the start of Phase II. Notably, no abnormal shifts in the peak particle diameter occurred during the injection period – the aerosol size distribution broadened slightly but the primary peak stayed near its expected size range, indicating that the aerosol detection continued to perform consistently even as concentration rose.

After slurry injection stopped, the system reached a steady state. In Phase II, the particle size distribution remained stable and showed minimal change over the ensuing 24 h. As illustrated by the latter half of Fig. 9b, the contour plot exhibits a flat profile – the particle count and size distribution did not drift, demonstrating that the measurement had reached equilibrium. This confirms that after the buildup in Phase I, the slurry's particle population in the tank was maintained uniformly (with the help of continuous mixing) and the measurement system did not suffer from any noticeable baseline drift or fouling over time.

Fig. 9c compares the ASD and DF-corrected HPSD obtained by the algorithm at three representative points during Phase I (corresponding to dilution factors DF = 2497, 1753, and 1002 at early, mid, and late injection, respectively). In each case, the ASD contained a prominent NVR artifact in the smaller size range, which the algorithm successfully removed to yield the hydrosol particle size distribution (HPSD). The DF-corrected HPSD curves at these three dilutions all exhibit a primary mode around 70 nm, confirming that the instrument and algorithm consistently identify the main silica particle peak across the injection

period. However, the HPSD amplitude at the mode diameter decreased with increasing concentration (i.e., with decreasing DF) even if the HPSDs are DF-corrected. Ideally, DF correction would yield similar peak amplitudes across dilutions, but at high solids loading the aerosolization step promotes multiplet formation: multiple particles are entrained into a single atomized droplet and, upon drying, are detected as a larger particle rather than as separate singles. This effect redistributes number concentration from the mode to slightly larger diameters, producing a more pronounced right-hand shoulder in the HPSD as shown in enlarged plot in Fig. 9c. Consequently, the value at the mode bin of DF × $dN_{HP}/d\log_{10}D_p$ decreases over concentration increase and the mode position itself remains essentially unchanged. Fig. S3 presents the multi-mode lognormal fittings for selected nine cases via long-term measurement, including the three DFs shown in Fig. 9c along with the corresponding NVR–particle separation results.

For comparison, DLS measurements were performed and the intensity-weighted DLS distributions (overlaid in Fig. 9c) appear broadened and shifted toward larger diameters relative to the number-based HPSD – an expected outcome due to the disproportionate scattering contribution of larger particles as discussed earlier in results of other slurry samples.

Over the long-term test for 48 h, the A-SMPS performed nearly 1000 consecutive scans, providing a rich dataset to evaluate consistency. Fig. 10a summarizes the time trends of the DF and the N_{HP} derived by algorithm, and includes the DF-corrected original number concentration (DF × N_{HP}) as green scatter. As slurry injection progressed in Phase I, the DF (blue dashed line) decreased from ~ 3 × 10^5 toward ~ 800, reflecting the increasing fraction of slurry in the tank. Plotted alongside is the fractional concentration (1/DF), normalized to its maximum value (red solid line), and the normalized N_{HP} obtained from each SMPS scan (red circular markers). The measured N_{HP} closely tracked the injection fraction over time: during Phase I, N_{HP} plots rise in tandem with the normalized fractional concentration (normalized 1/DF) curve, indicating that the aerosol-to-hydrosol inversion algorithm accurately captures the growth in particle concentration. The linear relationship is quantified in Fig. 10b, which shows N_{HP} versus 1/DF for all Phase I data. A best-fit line yields a coefficient of determination R^2 = 0.997, essentially a unity correlation. This excellent linearity demonstrates that, within the tested range, the system's response is directly proportional to the slurry fraction in the mixture. In other words, no significant biases or saturation effects emerged as concentration increased – a strong validation of both the SMPS measurement fidelity and the algorithm-based DF correction scheme over long durations.

During the 24-hour post-injection period (i.e., Phase II), the dilution factor remained fixed at DF ≈ 804 (the final dilution of the slurry in the tank). The SMPS continued to scan the recirculating sample, yielding an essentially constant N_{HP} over time. Fig. 10c compiles the Phase II N_{HP} data as a box-plot to assess measurement reproducibility. The average N_{HP} was found to be 2.42 × 10^{11} ml^{-1} with a coefficient of variation (CV) of only 3.37 % across ~ 500 scans in Phase II. This very low variation confirms that the particle concentration remained steady and that the measurement system did not exhibit any appreciable drift, noise escalation, or clogging over 24 h of continuous operation. Such stability is crucial for industrial monitoring, and here it indicates that the atomizer, SMPS, and associated hardware maintained consistent performance throughout prolonged use.

For quantitative description of the long-term experiment results, we divided the data into several time and dilution-factor ranges and analyzed the correlation and stability metrics as listed in Table 2. This breakdown highlights how the measurement system performs from the initial ultra-dilute condition through the steady-state phase. At start-up (UPW to DF ≈ 10,000; 0 to 2.1 h), the system operated in a detection-limited regime: the 1/DF-N_{HP} correlation was negligible (R^2 ≈ 0), and the DF-corrected original concentration (DF × N_{HP}, green scatter in Fig. 10a) was highly scattered (average 2.38 × 10^{14} ml^{-1}, SD 6.44 × 10^{14} ml^{-1} and CV 269.99 %), indicating the dominance of background noise (e.g., NVRs) over reliable particle detection. As injection progressed (UPW to DF ≈ 3,000; 0 to 6.4 h), the slurry signal began to emerge and the correlation improved (R^2 = 0.646), though variability in DF × N_{HP} remained large (CV 183.60 %), consistent with comparatively low particle counts. Once the slurry fraction clearly dominated (Phase I, DF ≈ 10,000 to 804; 2.1 to 25 h), the system exhibited near-unity behavior as N_{HP} scaled linearly with fractional concentration (R^2 = 0.994), while DF × N_{HP} stabilized at approximately constant levels (average 1.91 × 10^{14} ml^{-1}, SD 0.16 × 10^{14} ml^{-1} and CV 8.47 %). This trend was even stronger in the latter injection segment (DF ≈ 3,000 to 804; 6.5 to 25 h), with R^2 = 0.989 and very low scatter (average 1.97 × 10^{14} ml^{-1}, SD 0.06 × 10^{14} ml^{-1}, CV 3.06 %), demonstrating high-fidelity tracking and minimal bias.

During Phase II at fixed DF ≈ 804 (25 to 48 h), the recirculating

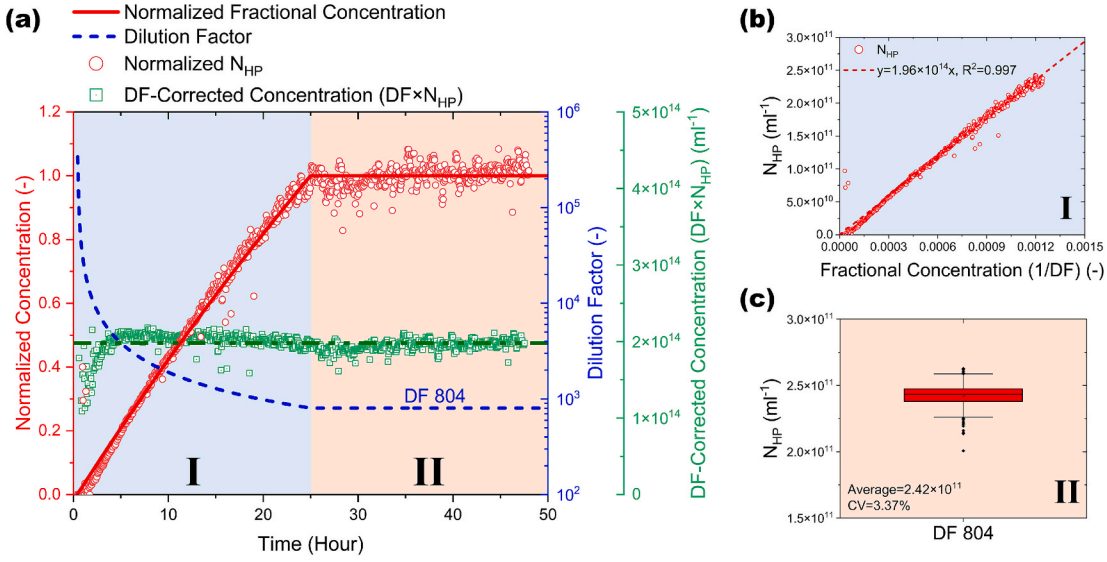

Fig. 10. Data analysis of long-term Silica slurry 2 data under constant-flow-rate slurry injection and post-injection stabilization: (a) time-dependent plot of dilution factor (blue dashed line), normalized fractional concentration (red line), normalized N_{HP} from each SMPS scan (red scatter), and DF-corrected original number concentration (DF × N_{HP}, green scatter) obtained by algorithm; (b) linear correlation between fractional concentration (1/DF) and N_{HP} in Phase I (R^2 = 0.997); (c) box-plot of N_{HP} in Phase II (DF = 804) showing high reproducibility with an average N_{HP} of 2.42 × 10^{11} ml^{-1} and a coefficient of variation (CV) of 3.37 %.

Table 2
Quantitative evaluation of concentration linearity and long-term stability across dilution-factor ranges in the 48-hour continuous-flow test.

Dilution Factor Range	Time (Hour)	1/DF vs N_{HP}	DF × N_{HP}		
		R^2 (–)	Average ($\times 10^{14}$ ml^{-1})	Standard Deviation ($\times 10^{14}$ ml^{-1})	CV (%)
UPW ~ DF 10000	0 ~ 2.1	0.000	2.38	6.44	269.99
UPW ~ DF 3000	0 ~ 6.4	0.646	1.88	3.45	183.60
DF 804 (Phase II)	25 ~ 48	–	1.95	0.07	3.37
DF 10000 ~ DF 804 (End of Phase I)	2.1 ~ 25	0.994	1.91	0.16	8.47
DF 10000 ~ DF 804 (Phase II Included)	2.1 ~ 48	–	1.93	0.13	6.46
DF 3000 ~ DF 804 (End of Phase I)	6.5 ~ 25	0.989	1.97	0.06	3.06
DF 3000 ~ DF 804 (Phase II Included)	6.5 ~ 48	–	1.96	0.064	3.26

system reached a steady state: N_{HP} remained essentially constant, as summarized by the box plot in Fig. 10c, with an average of 2.42 × 10^{11} ml^{-1} and CV 3.37 % across ~ 500 scans. Consistently, the DF-corrected original concentration in Fig. 10a (green scatter) stayed approximately constant (average 1.95 × 10^{14} ml^{-1}, SD 0.07 × 10^{14} ml^{-1}, CV 3.37 %), indicating no discernible drift or fouling over 24 h of continuous operation. Over extended windows that include Phase II, DF × N_{HP} remained effectively invariant: 1.93 × 10^{14} ml^{-1} (SD 0.13 × 10^{14} ml^{-1}, CV 6.46 %) for 2.1 to 48 h (DF ≈ 10,000 to 804 to constant) and 1.96 × 10^{14} ml^{-1} (SD 0.06 × 10^{14} ml^{-1}, CV 3.26 %) for 6.5 to 48 h (DF ≈ 3,000 to 804 to constant).

To articulate an uncertainty budget for the measurement and algorithm system, we consider the major sources of measurement uncertainty – including counting statistics at low concentrations, potential biases from particle multiplet formation at high concentrations, calibration accuracy of the SMPS (via PSL standards), and any drift in the aerosol generation or detection system over time. The 48-hour continuous experiment enables quantification of these factors. In the initial ultra-dilute stage of the long-term test, measurement noise dominated (reflected by high variability, CV > 100 % when DF ≈ 10,000), but once the particle concentration rose into the optimal range, the system's response became highly linear and predictable (with R2 ≈ 0.99 for 1/DF-N_{HP} correlation). During the steady-state phase at DF ≈ 804, the number concentration remained essentially constant with a coefficient of variation of only ~ 3.3 % over ~ 500 scans, indicating excellent repeatability of the measurement system. Importantly, no systematic drift in particle count or peak size was observed over 24 h of continuous operation, evidencing negligible instrumental drift or algorithmic bias accumulation. Based on these results, we estimate the expanded uncertainty (at 95 % confidence) of the particle concentration measurement to be on the order of only a few percent under well-controlled conditions. Similarly, the uncertainty in particle size (e.g., mode diameter) is very small – the main peak position varied by at most a few nanometers between measurements at different DFs and over time. In summary, our method's uncertainty budget is dominated by statistical noise at the extremes of concentration, but within the normal operating range it achieves high accuracy and precision. The observed reproducibility across dilution factors and over prolonged monitoring demonstrates that the aerosol-to-hydrosol inversion process is metrologically sound, with performance well within the requirements for quantitative nanoparticle size distribution measurements.

Taken together, these results show that beyond the initial detection-limited interval, the system provides a linear response to concentration changes (Phase I; $R^2 \approx 0.99$) and stable, quantitative recovery of the original concentration over many hours, with low scatter (CV of a few percent). The near-horizontal DF × N_{HP} trend in Fig. 10a and the interval statistics in Table 2 jointly confirm that the A-SMPS and inversion algorithm deliver accurate, drift-free concentration monitoring suitable for long-term CMP slurry applications. The same maintenance routine applied in shorter measurements was also followed for the long-term stability test, and no abnormal trends or performance degradation were observed. This result indicates that the established maintenance protocol was effective in preserving the system's stability and cleanliness even during extended continuous operation.

7. Conclusion

This study established a comprehensive framework that integrates aerosol measurement and hydrosol inversion to quantitatively characterize colloidal nanoparticles in liquid suspensions such as CMP slurries. The proposed atomizer–SMPS (A-SMPS) configuration, combined with a multi-stage inversion algorithm, reliably converts aerosol particle size distributions (ASDs) into NVR-subtracted hydrosol particle size distributions (HPSDs) while accurately reconstructing the original liquid-phase concentration.

Through calibration using monodisperse PSL standards, the algorithm determined a size-dependent correlation between aerosol and hydrosol number concentrations, enabling precise compensation for transmission losses during aerosolization. A multi-modal fitting procedure with a 10 % geometric-mean merging threshold and slope-based classification was developed to isolate the genuine particle modes from non-volatile-residue (NVR) artifacts. This combination successfully removed spurious peaks and ensured that the retrieved HPSDs represent only the true particle population.

Experimental validation using industrial-grade ceria- and silica-based CMP slurries across multiple dilution factors confirmed the method's reliability. After applying the inversion and dilution factor correction, the DF-corrected HPSDs from different samples nearly overlapped, indicating accurate recovery of the undiluted particle distribution.

Quantitatively, the DF-corrected original number concentration (DF × N_{HP}) remained constant within a few percent variation, and the N_{HP}–1/DF regressions yielded $R^2 \approx 1$, verifying both linearity and concentration conservation. A 48-hour long-term stability test further demonstrated the robustness of the measurement system and algorithm. During continuous operation with an industrial Silica slurry (referred to as Silica Slurry 2), the particle concentration scaled linearly with dilution during injection ($R^2 = 0.997$) and remained stable during 24 h of steady-state circulation (CV ≈ 3.3 % across ~ 500 scans) without any observable drift, clogging, or signal loss. This confirms that the A-SMPS system can sustain prolonged, drift-free monitoring while maintaining mechanical and metrological stability.

Overall, this work extends aerosol-based metrology to quantitative liquid-phase nanoparticle characterization. By integrating NVR subtraction, size-dependent calibration, and DF-correction logic, the proposed method achieves accurate, reproducible, and metrologically traceable hydrosol particle size analysis. The A-SMPS framework therefore provides a robust, high-throughput, and industrially adaptable alternative to conventional optical techniques, offering practical potential for real-time CMP slurry monitoring and broader hydrosol applications in nanoparticle process control.

Declaration of generative AI and AI-assisted technologies in the manuscript preparation process

During the preparation of this work, the author(s) used ChatGPT (OpenAI) for three purposes: (1) to refine sentence structure and verify expressions during manuscript writing, (2) to assist in debugging code during algorithm development, and (3) to proofread and check English grammar after the manuscript was completed. After using this tool, the author(s) carefully reviewed and edited the content to ensure accuracy and originality, and take full responsibility for the content of the published article.

CRediT authorship contribution statement

Seongmin Cho: Writing – original draft, Visualization, Validation, Software, Methodology, Investigation, Formal analysis, Data curation, Conceptualization. **Yongjae Cho:** Resources, Methodology, Data curation. **Yusun Lee:** Methodology. **Seungjae Gwak:** Resources. **Heedo Seo:** Formal analysis, Investigation. **Su Bin Min:** Resources, Investigation. **Young June Won:** Validation, Investigation. **Jung-Hun Noh:** Resources. **Handol Lee:** Writing – review & editing, Resources. **Dong-Bin Kwak:** Writing – review & editing, Supervision, Project administration, Funding acquisition, Conceptualization.

Declaration of competing interest

The authors declare that they have no known competing financial interests or personal relationships that could have appeared to influence the work reported in this paper.

Acknowledgement

This paper was supported by Korea Institute for Advancement of Technology (KIAT) grant funded by the Korea Government (MOTIE) (RS-2025-02304112, HRD Program for Industrial Innovation).

Appendix A. Supplementary data

Supplementary data to this article can be found online at https://doi.org/10.1016/j.measurement.2025.119624.

Data availability

Data will be made available on request.

References

[1] O.V. Salata, Applications of nanoparticles in biology and medicine, J. Nanobiotechnol. 2 (2004) 3.
[2] Y. Fan, M. Marioli, K. Zhang, Analytical characterization of liposomes and other lipid nanoparticles for drug delivery, J. Pharm. Biomed. Anal. 192 (2021) 113642.
[3] E.R. Waclawik, J. Chang, A. Ponzoni, I. Concina, D. Zappa, E. Comini, N. Motta, G. Faglia, G. Sberveglieri, Functionalised zinc oxide nanowire gas sensors: Enhanced NO2 gas sensor response by chemical modification of nanowire surfaces, Beilstein J. Nanotechnol. 3 (2012) 368–377.
[4] F. Rodríguez-Mas, J.C. Ferrer, J.L. Alonso, D. Valiente, S. Fernández de Ávila, A Comparative Study of Theoretical Methods to Estimate Semiconductor Nanoparticles' size, Crystals (2020).
[5] A.M. Golsheikh, K.Z. Kamali, N.M. Huang, A.K. Zak, Effect of calcination temperature on performance of ZnO nanoparticles for dye-sensitized solar cells, Powder Technol. 329 (2018) 282–287.
[6] C.S.C. Santos, B. Gabriel, M. Blanchy, O. Menes, D. García, M. Blanco, N. Arconada, V. Neto, Industrial Applications of Nanoparticles – A Prospective Overview, Materials Today: Proceedings, 2 (2015) 456–465.
[7] L. Zhang, X. Lu, A.A. Busnaina, The role of carboxylic acids on nanoparticle removal in post CMP cleaning process for cobalt interconnects, Mater. Chem. Phys. 275 (2022) 125199.
[8] D. Speed, P. Westerhoff, R. Sierra-Alvarez, R. Draper, P. Pantano, S. Aravamudhan, K.L. Chen, K. Hristovski, P. Herckes, X. Bi, Y. Yang, C. Zeng, L. Otero-Gonzalez, C. Mikoryak, B.A. Wilson, K. Kosaraju, M. Tarannum, S. Crawford, P. Yi, X. Liu, S. V. Babu, M. Moinpour, J. Ranville, M. Montano, C. Corredor, J. Posner, F. Shadman, Physical, chemical, and in vitro toxicological characterization of nanoparticles in chemical mechanical planarization suspensions used in the semiconductor industry: towards environmental health and safety assessments, Environ. Sci. Nano 2 (2015) 227–244.
[9] R.D. Boyd, S.K. Pichaimuthu, A. Cuenat, New approach to inter-technique comparisons for nanoparticle size measurements; using atomic force microscopy, nanoparticle tracking analysis and dynamic light scattering, Colloids Surf A Physicochem Eng Asp 387 (2011) 35–42.
[10] X. Luan, Y. Liu, B. Zhang, S. Wang, X. Niu, C. Wang, J. Wang, Investigation of the barrier slurry with better defect performance and facilitating post-CMP cleaning, Microelectron. Eng. 170 (2017) 21–28.
[11] N.C. Crawford, S.K.R. Williams, D. Boldridge, M.W. Liberatore, Shear thickening and defect formation of fumed silica CMP slurries, Colloids Surf A Physicochem Eng Asp 436 (2013) 87–96.
[12] Z. Jia, J. Li, L. Gao, D. Yang, A. Kanaev, Dynamic Light Scattering: a Powerful Tool for In Situ Nanoparticle Sizing, Colloids and Interfaces (2023).
[13] J. Lim, S.P. Yeap, H.X. Che, S.C. Low, Characterization of magnetic nanoparticle by dynamic light scattering, Nanoscale Res. Lett. 8 (2013) 381.
[14] R. Pecora, Dynamic Light Scattering Measurement of Nanometer Particles in Liquids, J. Nanopart. Res. 2 (2000) 123–131.
[15] C.M. Hoo, N. Starostin, P. West, M.L. Mecartney, A comparison of atomic force microscopy (AFM) and dynamic light scattering (DLS) methods to characterize nanoparticle size distributions, J. Nanopart. Res. 10 (2008) 89–96.
[16] J. Lee, S. He, G. Song, C.J. Hogan, Size distribution monitoring for chemical mechanical polishing slurries: an intercomparison of electron microscopy, dynamic light scattering, and differential mobility analysis, Powder Technol. 396 (2022) 395–405.
[17] J. Ye, J. Liu, J. Ren, J. Lu, Y. Liu, The investigation of traceable preparation technique of submicron particle number concentration standards in liquids, Powder Technol. 444 (2024) 120043.
[18] M.A. Rahman, Q. Ou, D. Pui, Electrospray-Scanning Mobility Particle Sizer (ES-SMPS) Technique: Superior Sizing and Multimodal Characterization of Colloidal Nanoparticles Compared to NTA and DLS, Anal. Chem. 96 (2024) 18946–18956.
[19] D.M. Knotter, S.A.M. Wolters, M.A. Kasanrokijat, Particle Concentration Measurements in Process Liquids Using Light-Scattering Techniques, Particulate Science and Technology, 25 (2007) 435–447.
[20] B. Dash, K. Iyer, J. Barker, S. Chakravorty, Dynamic Dispatching for FOUP Cleaning, 2020 31st Annual SEMI Advanced Semiconductor Manufacturing Conference (ASMC), 2020, pp. 1–4.
[21] D. Florescu, D.R. Rodier, B.A. Knollenberg, Chapter 12 - Detection and Measurement of Particulate Contaminants, in: K.A. Reinhardt, W. Kern (Eds.), Handbook of Silicon Wafer Cleaning Technology (third Edition), William Andrew Publishing, 2018, pp. 659–699.
[22] A. Matter, A. Koulov, S. Singh, H.-C. Mahler, H. Reinisch, C. Langer, B. Zucol, R. Mathaes, Variance between Different Light Obscuration and Flow Imaging Microscopy Instruments and the Impact of Instrument Calibration, J. Pharm. Sci. 108 (2019) 2397–2405.
[23] M. Bismuth, M. Eck, T. Ilovitsh, Nanobubble-mediated cancer cell sonoporation using low-frequency ultrasound, Nanoscale 15 (2023) 17899–17909.
[24] H. Shinar, T. Ilovitsh, Volumetric Passive Acoustic Mapping and Cavitation Detection of Nanobubbles under Low-Frequency Insonation, ACS Mater. Au 5 (2025) 159–169.
[25] V. Uskoković, Dynamic Light Scattering based Microelectrophoresis: Main prospects and Limitations, J. Dispers. Sci. Technol. 33 (2012) 1762–1786.
[26] H. Lee, D.-B. Kwak, S.C. Kim, D.Y.H. Pui, Characterization of colloidal nanoparticles in mixtures with polydisperse and multimodal size distributions using a particle tracking analysis and electrospray-scanning mobility particle sizer, Powder Technol. 355 (2019) 18–25.
[27] H. Lee, S.-C. Chen, C. Kim, E. Westenburg, S.I. Moon, D.Y.H. Pui, Evaluation of concentration measurement techniques of colloidal nanoparticles for microfiltration and ultrafiltration applications: Inductively coupled plasma-mass spectrometry, nanoparticle tracking analysis and electrospray-scanning mobility particle sizer, Sep. Purif. Technol. 184 (2017) 34–42.
[28] H. Lee, D.-B. Kwak, S.C. Kim, Q. Ou, D.Y.H. Pui, Influence of colloidal particles with bimodal size distributions on retention and pressure drop in ultrafiltration membranes, Sep. Purif. Technol. 222 (2019) 352–360.
[29] S. Jeon, D.R. Oberreit, G. Van Schooneveld, C.J. Hogan, Nanomaterial size distribution analysis via liquid nebulization coupled with ion mobility spectrometry (LN-IMS), Analyst 141 (2016) 1363–1375.
[30] D. Kwak, J. Kim, S. Oh, C. Bae, T. Kim, Size distribution measurement of mixed abrasive slurry for chemical mechanical planarization using an electrospray scanning mobility particle sizer, Colloids Surf A Physicochem Eng Asp 674 (2023) 131798.
[31] C. Shin, J. Choi, D. Kwak, J. Kim, J. Yang, S.-K. Chae, T. Kim, Evaluation of size distribution Measurement Methods for Sub-100 nm Colloidal Silica Nanoparticles and its Application to CMP Slurry, ECS J. Solid State Sci. Technol. 8 (2019) P3195.
[32] D. Kwak, J. Kim, S. Oh, C. Bae, T. Kim, Application of electrospray-scanning mobility particle sizer for the measurement of sub-10 nm chemical mechanical planarization slurry abrasive size distribution, Rev. Sci. Instrum. 91 (2020) 075117.
[33] A. Wiedensohler, W. Birmili, A. Nowak, A. Sonntag, K. Weinhold, M. Merkel, B. Wehner, T. Tuch, S. Pfeifer, M. Fiebig, A.M. Fjäraa, E. Asmi, K. Sellegri, R. Depuy, H. Venzac, P. Villani, P. Laj, P. Aalto, J.A. Ogren, E. Swietlicki, P. Williams, P. Roldin, P. Quincey, C. Hüglin, R. Fierz-Schmidhauser, M. Gysel, E. Weingartner, F. Riccobono, S. Santos, C. Grüning, K. Faloon, D. Beddows, R. Harrison, C. Monahan, S.G. Jennings, C.D. O'Dowd, A. Marinoni, H.G. Horn, L. Keck, J. Jiang, J. Scheckman, P.H. McMurry, Z. Deng, C.S. Zhao, M. Moerman,

B. Henzing, G. de Leeuw, G. Löschau, S. Bastian, Mobility particle size spectrometers: harmonization of technical standards and data structure to facilitate high quality long-term observations of atmospheric particle number size distributions, Atmos, Meas. Tech. 5 (2012) 657–685.
[34] I. Hwang, K.-H. Ahn, Performance evaluation of conventional type conductive cooling continuous flow compact water-based CPC (Hy-WCPC), J. Aerosol Sci 113 (2017) 12–19.
[35] C. Qi, P. Kulkarni, Miniature differential mobility analyzer for compact field-portable spectrometers, Aerosol Sci. Tech. 50 (2016) 1145–1154.
[36] D.-W. Lee, N.-H. Kim, E.-G. Chang, Effect of nonionic surfactants on the stability of alumina slurry for Cu CMP, Mater. Sci. Eng. B 118 (2005) 293–300.
[37] S. Cho, D.-B. Kwak, D.Y.H. Pui, Impact of high-altitude conditions and low ambient pressure on saliva evaporation rate and airborne transmission of viruses, Build. Environ. 269 (2025) 112453.
[38] D.-B. Kwak, S.C. Kim, H. Lee, D.Y.H. Pui, Numerical investigation of nanoparticle deposition location and pattern on a sharp-bent tube wall, Int. J. Heat Mass Transf. 164 (2021) 120534.
[39] W.C. Hinds, Y. Zhu, Aerosol technology: properties, behavior, and measurement of airborne particles, John Wiley & Sons, 2022.
[40] X.L. Chu, A.D. Nikolov, D.T. Wasan, Effects of Particle size and Polydispersity on the Depletion and Structural Forces in Colloidal Dispersions, Langmuir 12 (1996) 5004–5010.
[41] A. Othman, H.J. Kim, R. Trivedi, T. Kulasingam, J. Seo, Understanding and mitigating temperature-induced agglomeration in silica-based chemical mechanical planarization (CMP) slurry storage, Colloids Surf A Physicochem Eng Asp 691 (2024) 133802.